Distribution Agreement

In presenting this thesis as a partial fulfillment of the requirements for a degree from Emory University, I hereby grant to Emory University and its agents the non-exclusive license to archive, make accessible, and display my thesis in whole or in part in all forms of media, now or hereafter now, including display on the World Wide Web. I understand that I may select some access restrictions as part of the online submission of this thesis. I retain all ownership rights to the copyright of the thesis. I also retain the right to use in future works (such as articles or books) all or part of this thesis.

Fan (Raymond) Fei   March 22, 2023

Engineering CXCL13 Secreting CAR T Cells for Ovarian Cancer

By

Fan Fei

Sarwish Rafiq, PhD
Adviser

Biology

Sarwish Rafiq, PhD
Adviser

Eliver Ghosn, PhD

Committee Member

Rui Kong, PhD

Committee Member

Rustom Antia, PhD

Committee Member

2023

Engineering CXCL13 Secreting CAR T Cells for Ovarian Cancer

By

Fan Fei

Sarwish Rafiq, PhD

Adviser

An abstract of
a thesis submitted to the Faculty of Emory College of Arts and Sciences of Emory University
in partial fulfillment
of the requirements of the degree of
Bachelor of Science with Honors

Biology

2023

Abstract

Engineering CXCL13 Secreting CAR T Cells for Ovarian Cancer

By Fan Fei

As one of the leading causes of death in gynecological malignancies, ovarian cancers is mostly diagnosed in the late stage due to the lack of early detection tests and early symptoms[1,2]. By the time of diagnosis, majority of patients with ovarian cancer have developed metastasis in peritoneal cavity[3]. And even after standard surgery and chemotherapy, drug resistance and relapse are still very common[4]. Hence, developing new treatments, such as immune checkpoint inhibitors and cellular therapy, are urgently needed. In this study, we developed a novel CAR T cell therapy for ovarian cancer. High-grade serous ovarian cancer cells express elevated levels of tumor-associated antigen, Muc16CD[5]. We used anti-Muc16CD CAR to target the ectodomain of Muc16 for antigen recognition and tumor clearance. To engage the endogenous immune system and create a pro-inflammatory tumor microenvironment in ovarian cancers, we co-modified CAR T cells to express the B cell chemoattractant CXCL13 as armor on anti-Muc16CD CAR hoping to induce tertiary lymphoid structure formation at local tumor site. We propose that tertiary lymphoid structures help to select and activate tumor antigen-specific antibody-secreting cells and potentially attract other CXCR5+ endogenous immune cells. In this study, we engineered, validated, and tested the function of a novel CXCL13 expressing armored CAR T cells *in vitro* and have begun *in vivo* study to investigate the potential anti-tumor roles of CXCL13 and to compare CAR T cell functions between armored-CAR and CAR in a syngeneic mouse ovarian cancer model.

Engineering CXCL13 Secreting CAR T Cells for Ovarian Cancer

By

Fan Fei

Sarwish Rafiq, PhD

Adviser

A thesis submitted to the Faculty of Emory College of Arts and Sciences
of Emory University in partial fulfillment
of the requirements of the degree of
Bachelor of Science with Honors

Biology

2023

Acknowledgements

TABLE OF CONTENTS

1 Introduction

1.1 CAR T Cell Therapy

Chimeric antigen receptor (CAR) T cell therapy is currently one of the most studied immunotherapy treatments for cancers. Its antigen-specific targeting mechanism provides enhanced antitumor function while minimizing the common side effects, such as oxidative stress, genotoxicity, and carcinogenicity etc., resulting from chemotherapy and radiation therapies.[6] A T-cell receptor (TCR) will target a specific antigen through TCR-peptide/MHC interactions[7]. Unlike the TCR complex, a CAR can recognize an antigen due to a synthetic antigen recognition domain, which allows for MHC-independent activation **(Fig. 1)**. One of the most common antigen binding domains on a CAR is a single-chain variable fragment (scFv), which composes of the variable heavy and variable light chains on a monoclonal antibody[8,9]. This advantage of an scFv provides a lot of opportunities for tumor-associated antigen (TAA) selection. Alternative antigen binding domain like cytokines and nanobodies have also been investigated previously.
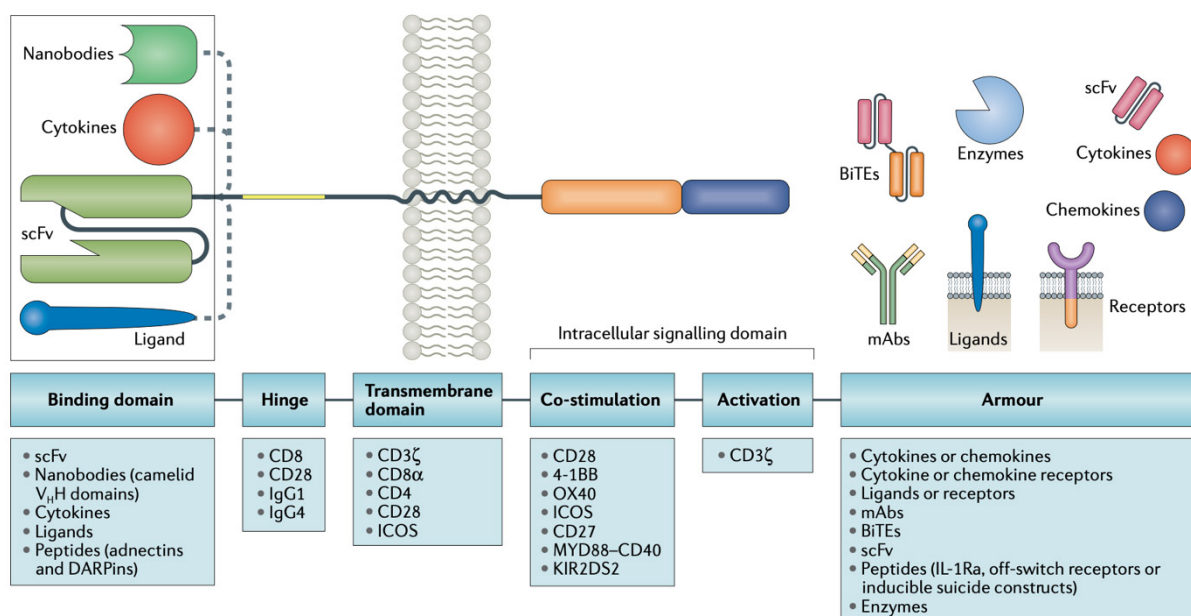

Fig.1 | Current Engineering Strategies to Design a CAR.[9]

CAR mainly composes of antigen binding domain, hinge, transmembrane domain, co-stimulatory domain, activation domain, and sometimes an armor. Different molecules being used on CAR contribute to different function and differentiation fate of the CAR T cells.

In addition to the antigen binding domain, a CAR T cell needs two other signals to be completely activated: a co-stimulatory signal and an activation signal. An endogenous TCR requires 3 signals to be fully activated: TCR-peptide/MHC signal, costimulatory signal, and cytokines[10]. Much like traditional T cell signaling, CD3ζ domain is required for CAR T cells to recruit intracellular signaling proteins to sustain T cell activation [11,12]. Co-stimulatory signal is also required to direct the functional outcome of T cell activation through different biochemical signalings[13]. Previous study has shown that CD28 costimulation domain amplifies the TCR signaling and induce T cells proliferation[14]. Another FDA-approved costimulation domain is 4-1BB. Both costimulatory domains confer different downstream signaling yet achieve similar clinical outsomes[15,16]. One of the few differences between CD28 and 4-1BB CAR is their difference in expansion kinetics. Zhao et al. reported that 1928z CAR T cells initially expand faster and eliminate more tumors in a Nalm6 leukemia mouse model, and 19BBz CAR T cells expand slower but outgrow the 1928z CAR T cells by day 14 and eventually achieve comparable tumor cells elimination[17]. Thus, CD28 costimulation domain confer greater functionality in terms of expansion, and 4-1BB constimulation domain confer greater persistence at a slower expansion rate, both of which achieve similar tumor elimination[17]. Additionally, CAR T cells with a CD28 costimulation domain are more likely to differentiate into effector memory T cells, while CAR T cells with a 4-1BB costimulation domain skew towards central memory T cells[18]. Lastly, to enhance the anti-tumor function of CAR T cells, CAR T cells can be engineered with an armor domain to help overcoming the

immunosuppressive signals in TME. In this study, we studied anti-Muc16CD CAR T cells with a CD28 costimulation domain, CD3ζ activation domain and chemokine CXCL13 armor.

Because of the unique design of incorporating all required T cell activation signals on one molecule, FDA-approved CAR T cell therapies have proven to be effective in controlling and even eradicating hematological malignancies. The novelty of CAR T cell therapy is within with the antigen recognition mechanism. yet the therapy has encountered impediments when targeting solid tumors[9,19]. Several reasons contribute to ineffective solid tumor clearance, including the presence of physical barrier that prevents CAR T cells infiltration, T cell inhibitory ligands presented on tumor cells, and the immunosuppressive cytokines and metabolites that are commonly overexpressed in the tumor microenvironment (TME)[20-23]. In the context of ovarian cancer, the immunosuppressive TME is contributed by immunoregulatory cells, such as cancer-associated fibroblast, myeloid-derived suppressor cell (MDSC), Treg, and M2 tumor-associated macrophage (TAM)[24]. This study specifically aims to reprogram the immunosuppressive TME in ovarian cancer by attracting CXCR5+ endogenous immune cells, such as CD4 and CD8 T cells, B cells. Attracted B cells and CD4 T cells could potentially induce tertiary lymphoid structures and positively select tumor antigen-specific B cells.

1.2 αMuc16CD CAR T Cell Therapy in Ovarian Cancer

Among various gynecological tumors, ovarian cancer has the highest mortality rate, and most patients have peritoneal metastasis at the time of diagnosis[25]. Different from other solid tumors that metastasize hematologically, ovarian cancer is more likely to metastasize to the peritoneum because ovary is in direct contact with the peritoneal cavity[26]. Ovarian cancer

often metastasizes to the peritoneum and omentum, which is why it is challenging to completely remove the tumor by surgery, and the treatment effect is usually limited[27,28]. In addition to surgery, treatment of ovarian cancer at present mainly relies on chemotherapy drugs, including cisplatin and paclitaxel, to achieve complete remission in patients. Although the recently developed therapy, such as targeted therapy, has prolonged the progression-free survival of patients, these drugs still have limited effect on prolonging the overall survival of patients[29,30]. Therefore, it is urgent to develop new therapy that can target the peritoneal metastasis of ovarian cancer. CAR T cell therapy has the potential to treat ovarian cancer because CAR T cells can directly recognize and kill the tumor cells in peritoneal cavity that are usually hard to be removed in surgery.

Courtesy of Heather K. Lin

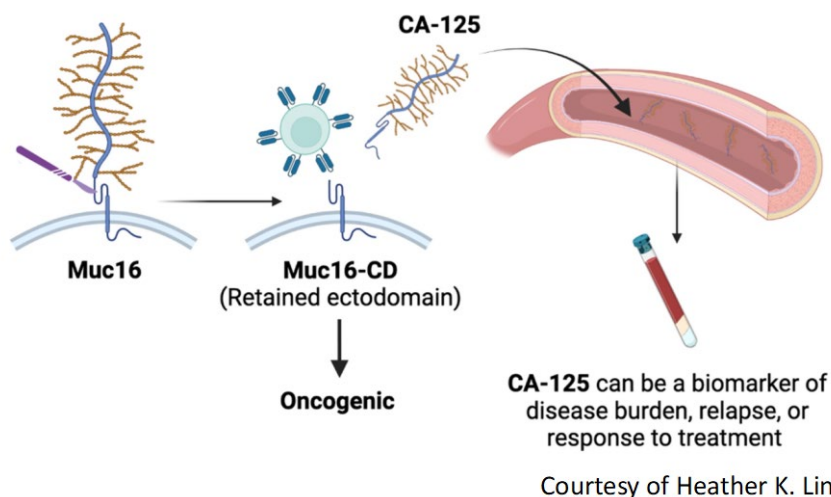**Fig.2 | Clinical Relevance of Antigen Muc16 in Ovarian Cancer**

The TAA we are targeting in this study is Muc16 from the mucin family glycoproteins. It is commonly overexpressed on ovarian and pancreatic tumor cells[5,31]. Because of the overexpression of Muc16 in ovarian cancer, the cleaved portion of Muc16 or CA-125 is a clinical marker for disease progression and relapse **(Fig. 2)**[32]. A novel scFv (4H11) was

previously developed to target against the retained ectodomain of Muc16 (Muc16CD) and has been previously validated in mouse ID8 ovarian cancer model[33-35].

1.3 CXCL13 Chemokine and Its Cognate Chemokine Receptor CXCR5

The chemokines are a family of proteins that signal through cell surface G protein-coupled heptahelical chemokine receptors and promote the migration of cells, specifically the leukocytes of immune system[36]. Chemokines' function of attracting various immune cells is important in regulating the development and homeostasis of the immune system[36]. For this reason, chemokines, in conjunction with cytokines and growth factors, are key regulators of immune response in the context of infection and cancer[37]. Chemokines can be structurally classified into four subfamilies (e.g., CXC, CC, C, and CX3C) by their positional arrangements of amino acid residue, cysteine[38]. Cysteine is structurally important for the chemokine families because the disulfide bonds formed by the cysteine residues stabilize the overall structure of the chemokine monomer[36,38]. In this study, we co-modified CAR T cells to express chemokine C-X-C motif ligand 13 (CXCL13), commonly known as B-cell chemoattractant. However, CXCL13 can also attract subsets of CD4 and CD8 T cells in the immune system via its cognate chemokine receptor CXCR5. Specific to CXCL13, CXCR5 can be activated and then transduce various downstream signaling pathways, including PI3K/Akt, MEK/ERK, and Rac pathways, to induce cellular chemotaxis[39,40]. Because CXCL13-CXCR5 axis can induce multiple pathways that are responsible for cell survival, proliferation, and migration, we hypothesize that CXCL13 can enhance CAR T cells' functionality by promoting survival and proliferation. Additionally, CXCL13 expressed by CAR T cells can

potentially interact with the endogenous immune system to create a pro-inflammatory tumor microenvironment **(Fig. 3)**.
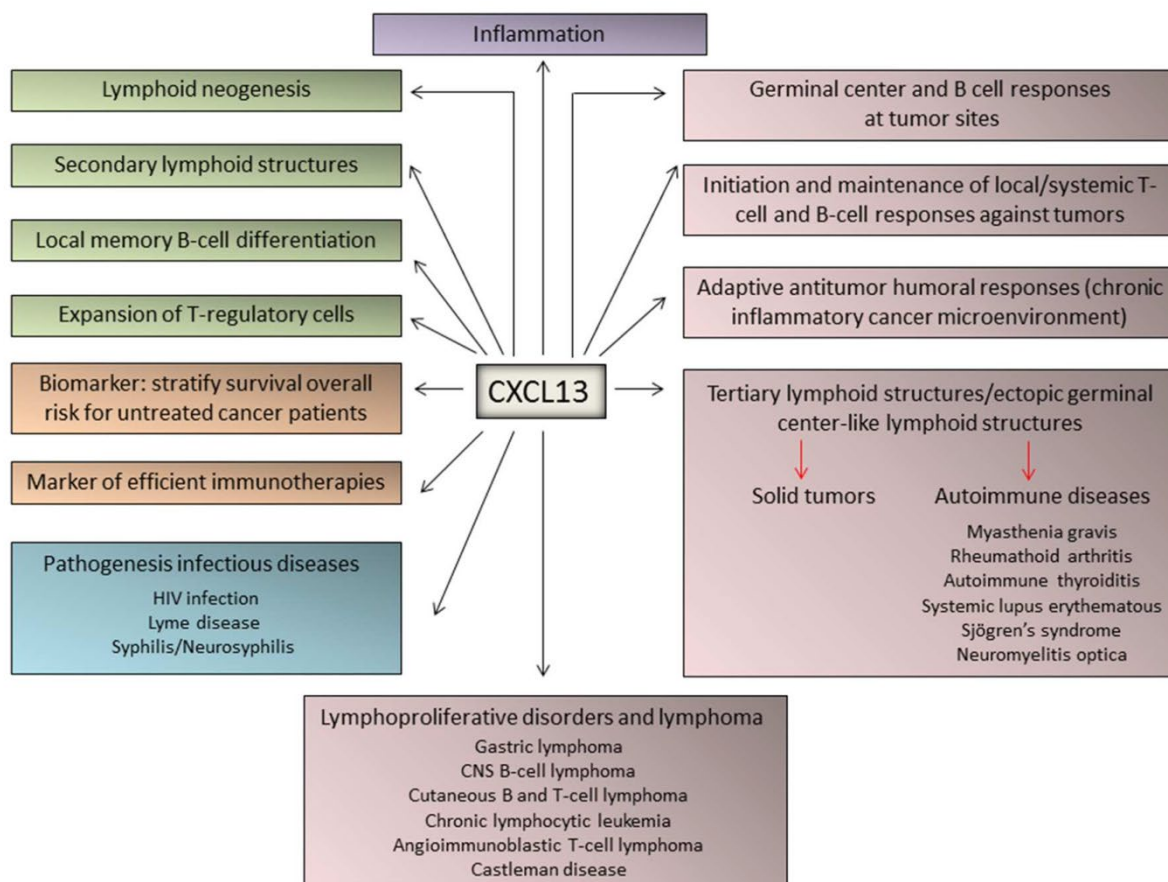
Fig.3 | CXCL13 has Potential Anti-tumor Function by Modulating T and B Cells Response and is Involved in Tertiary Lymphoid Structure Formation in Cancer[40].

In addition to CXCL13's physiological function of lymphoid neogenesis and B cell chemoattraction and pathological function in autoimmune disease, recent research have identified CXCL13 as a prognostic marker in immunotherapy and a molecule involved in tertiary lymphoid structure formation in cancer.

1.4 Tertiary Lymphoid Structure in Cancer

Tertiary lymphoid structure (TLS) is an organized structure composed of various immune cells that forms under chronic inflammation, such as chronic viral infection and cancer, inside the tissues[41]. Similar to the function of secondary lymphoid organ, B cells are selected

and activated within the TLS where they undergo somatic hypermutation and antibody class switching. Selected B cells can then differentiate into plasma cells that are capable of secreting TAA-specific antibodies and contribute to favorable clinical outcomes, including ovarian cancer[42,43]. Macrophages and natural killer (NK) cells can bind to the constant region of anti-tumor antibodies and cause antibody-dependent cellular cytotoxicity (ADCC) of tumor cells[44,45].

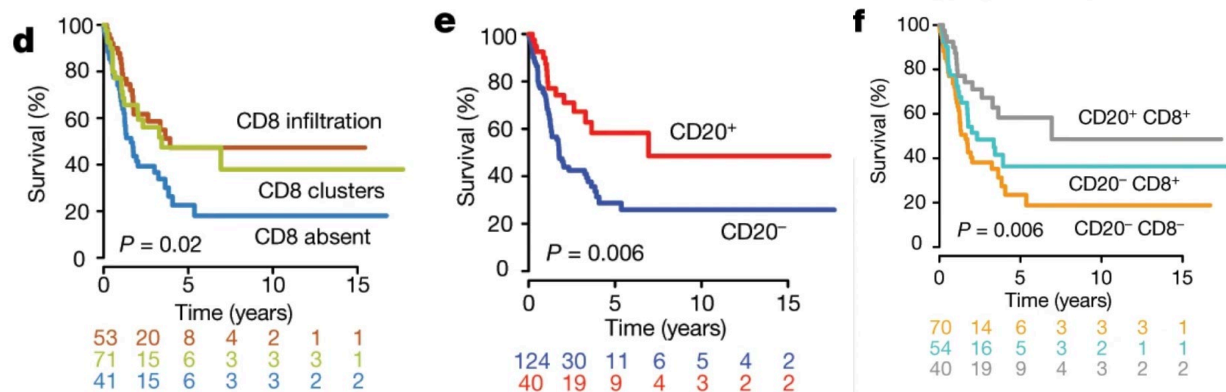**Fig.4 | Tumor-infiltrating CD8 T and CD20 B Cells Contribute to Better Prognosis in Solid Tumor, Melanoma[46]**
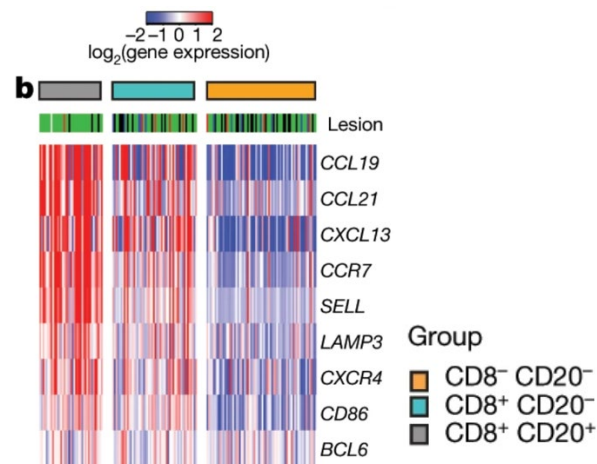

Fig.5 | CD8+ CD20+ TILs Group has Higher Level of TLS Gene Signatures, and CXCL13 is One of the TLS Gene Signatures[46]

In solid tumors, B cells play a key role in immunotherapy involved with immune checkpoint blockade (ICB). When studying the role of TLS in patients with melanoma, researchers first

ran immunohistochemistry analysis on patient samples and found that patients who have both CD20+ and CD8+ tumor infiltrating lymphocytes (TILs) achieve longer survival than patients who only have CD8+ TILs alone **(Fig. 4)**[46]. More importantly, the study also concludes that higher level of TLS gene signatures correctly predicts higher response to ICB in melanoma **(Fig. 5)**[46]. Additionally, Sorin et al. reported that CXCL13 can potentiate anti-PD-1 therapy by reducing the tumor volume in both HKP1 lung cancer model and MC38 colon cancer model[47].

In the context of ovarian cancer, tumor-infiltrating plasma cells are associated with presence of organized lymphoid aggregates (immature TLS) and a more robust cytolysis of CD8+ T cells and cytolysis-associated genes[48]. While this study did not further investigate the exact mechanism of how plasma cells work in concert with CD8+ T cells, the study did report that CD8+ T cells can exhibit more robust cytolysis when in the presence of plasma cells. Additionally, the study also characterized TLS into 4 different types from type I to type IV aggregates based on size, cellular composition, and degree organization. While type I aggregates (20-50 cells) is small and includes CD4+ and CD8+ T cells, B cells, and occasionally DC cells, type IV aggregates (100-300 cells) is large and includes clear organization of T and B cell zones and follicular DCs[48].
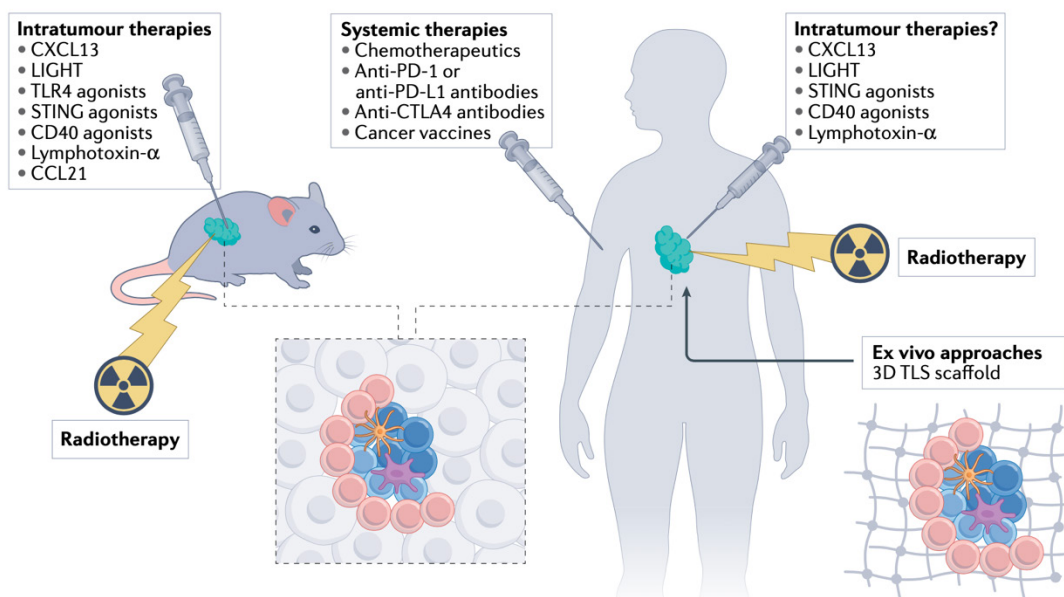
Fig.6 | Engineering Strategies to Induce TLS in Mouse Models and Cancer Patients[43]

In mouse cancer models, various immunostimulatory agents, such as TLR4 agonists, STING agonists, and CD40 agonists, and cytokine CXCL13 can induce TLS within the tumor tissue. In cancer patients, systemic treatment of immune checkpoint inhibitors, immunostimulatory agents, and chemokine can similarly induce TLS. In addition, radiotherapy and 3D biomaterial implants have also shown to induce TLS inside the tumor. In this study, we included CXCL13 as an armor on the CAR and to test the anti-tumor function of it hoping to see if CXCL13 from CAR T cells can similarly induce TLS.

In the TME, CXCL13 binds to chemokine receptor, CXCR5, and acts as a chemoattractant for both a subset of T cells and B cells, and colocalizes with the presence of tertiary lymphoid structures (TLS). CXCL13 and CD20 are two main markers for the detection of TLS in immunohistochemistry (IHC)[41]. Luther et al. have previously shown that ectopic expression of CXCL13 alone in pancreatic islets of transgenic mice can induce TLS that contains distinct structures comparable to a secondary lymph node[49]. Since presence of TLS oftentimes correlates with better clinical outcome in solid tumors, we hypothesized that CXCL13 chemoattractant will induce TLS formation in the context of CAR T cell therapy treating ovarian cancers **(Fig. 6)**.

1.5 Engineered CXCL13-secreting CAR in Ovarian Cancer

Because CXCL13 and B cells play an important and favorable role in ovarian cancer, we decided to use 4H11 scFv as our CAR model to design and engineer CXCL13-secreting 4H11 CAR to test the anti-tumor function of CXCL13[42]. As CXCL13 alone can induce TLS in transgenic mouse model and has anti-tumor functions in both human and mouse studies, this work aims to construct and validate the function of CXCL13-secreting CAR T cells *in vitro* and *in vivo*. We hypothesize that CXCL13 expressed by CAR T cells will bind to CXCR5 on CAR T cells and lead to improved CAR T cell function by inducing more IFN-g secretion, greater stimulation and proliferation capacity defined by expression levels of CD69 and Ki-67.

2 Materials and Methods

2.1 Molecular Cloning
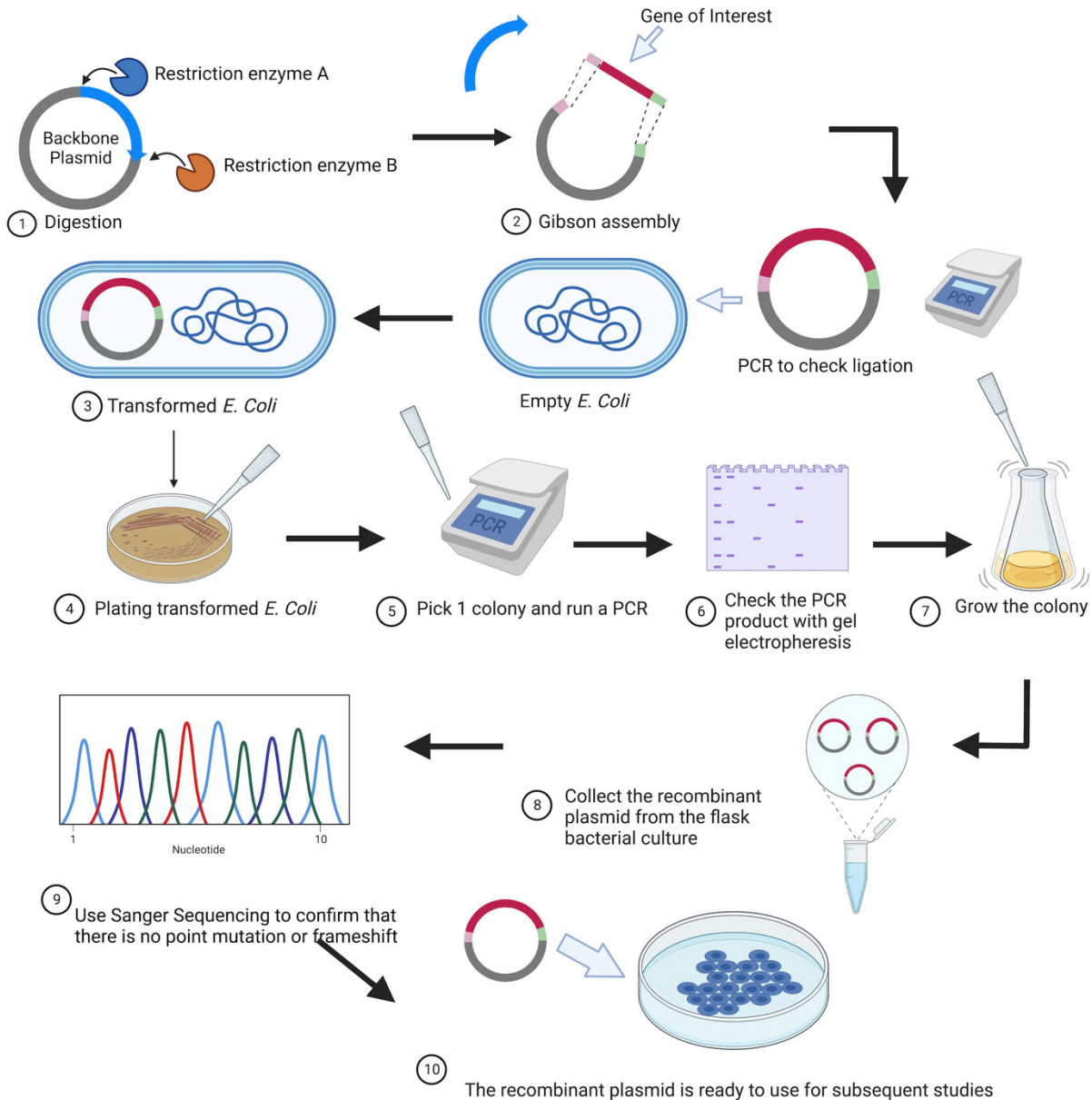
Fig. 7 | Schematic of Molecular Cloning for Constructing SFG Retroviral Backbone

Backbone was first chosen to design strategy of molecular cloning with compatible restriction enzymes and insert encoding for the gene of interest. For ligation, this study used Gibson assembly method which includes overlapping regions at both end of the inserts. PCR-validated construct will be transformed into E. coli for colony screening. Transformed colony was grown and collected using plasmid extraction. Extracted plasmid was again sequenced and validated prior to stable packaging cell manufacture.

2.2 H29 Transfection and Phoenix-ECO transduction in mouse T cells

We first chemically transfected the H29 cell with the vectors by using calcium chloride (CaCl2). After four days, we collected the viral supernatant from the H29 cell and removed the cells using a 0.45μm filter to transduce Phoenix-ECO packaging cells. Phoenix-ECO packaging cells contain gag-pol and envelope protein for ecotropic viruses[50]. The transduced Phoenix-ECO retroviral packaging cells were single-cell cloned by limiting dilution method. Flow cytometry was used to screen for a clone with 100% transduction efficiency. This clone was then used to transduce mouse T cells for CAR T cell manufacturing. H29 transfection is transient. H29s include the envelop and packaging elements for producing retrovirus. Transfected H29s will eventually lose the plasmid with gene of interest. Therefore, the gene of interest still need to be integrated to the genome for packaging cells to stably produce retrovirus. We collected retroviral supernatant from H29s cells and used it to transduce Phoenix-ECO that has built-in ecotropic envelop for infecting mouse T cells.

2.3 Flow Cytometry Analysis

We used APC- or FITC-conjugated primary antibody targeting against the scFv domain of the CAR. The conjugated primary antibody was titrated for optimal concentration per FACS tube before flow cytometry experiment. Sections 2.3, 2.6, 2.7, 2.8 can be combined. Remove redundant phrasing.

2.4 Mouse Splenocyte Isolation and T Cell Expansion and Transduction

Mouse spleen was isolated from female C57BL/6 mouse. Spleen was manually dissociated and filtered through cell strainer to obtain single cell suspension. Bulk splenocytes were treated with RBC lysis buffer (5mL) to deplete red blood cells. Splenocytes were washed in PBS and resuspended in RPMI media supplemented with 10% FBS and 3% ATOS. Con A (4

ug/uL) and rIL-2 (1.0U/mL) were added in resuspended splenocytes for mouse T cell expansion. Stimulated and expanded mouse T cells were transduced twice with filtered viral supernatant from Phoenix-ECO packaging cells for two consecutive days. Mouse T cells were supplemented with rIL-2 (1.0U/mL) on the day 4. Mouse T cell transduction was checked on the day 5 on flow cytometer. Only transduced T cells with higher than 20% transduction efficiency was used for downstream *in vitro* assays.

2.5 Luciferase-based Cytotoxicity Assay

Muc16CD+ and eGFP+ tumor cell lines were used for this experiment. CAR T cells and tumor cells were stained with trypan blue and counted on Bio-Rad automated cell counter. CAR T cells and tumor cells were co-cultured in a black-walled, clear bottom 96-well plate at an E:T ratio of 1:1, 1:3, 1:10, 1:20, and 1:30. Each condition has three replicates. At 48-hour or 72-hour timepoint, luciferin (2mM/well) was added into each well. Luminescence was read on BioTek Synergy Microplate Reader. The following formula was used to calculate % lysis:

$$\% \text{ Lysis} = \left(1 - \left(\frac{\text{sample}}{\text{tumor alone average}}\right)\right) * 100.$$

2.6 Intracellular Staining Flow Cytometry

Cells were collected from plate at 24 hours post coculture. Cells were washed in pure PBS and stained with Live/Dead Violet fixable viability dye for 30 minutes. BD Cytofix/Cytoperm Fixation/Permeabilization Solution kit was used to fix and permeabilize collected cells, according to manufacturer instructions. Fixed/permeabilized cells were incubated overnight with previously titrated antibodies and then washed twice with FACS buffer (PBS solution with 2.5% FBS) prior to flow cytometry analysis.

2.7 Cytokine Assay (IFN-g and IL-2)

CAR T cells and Muc16CD+ tumor cells were co-cultured at a 1:1 E:T ratio for 24 hours. At 20 hours, GolgiStop (0.5ul/ml) was added for optimal cytokine intracellular staining. Collected cells were fixed and permeabilized following the above-mentioned method prior to antibody staining. PE anti-mIFN-g and BV605 anti-mIL-2 were used to stain IFN-g and IL-2 in CD3+ CAR+ T cells. Cytokine levels were quantified in both median fluorescence intensity (MFI) and % of cells from intracellular staining flow cytometry.

2.8 Activation and Proliferation Assay (CD69 and Ki-67)

CAR T cells and Muc16CD+ tumor were co-cultured at a 1:1 E:T ratio for 24 hours. Cells for CD69 surface staining were washed twice, stained with PE anti-mCD69 for 30 minutes, and washed twice prior to flow cytometry analysis. The cells for Ki-67 intracellular staining were stained with fixable viability dye and fixed and permeabilized following the above-mentioned method. The cells were fixed and permeabilized and then stained with PerCP-Cyanine5.5 anti-mKi-67 overnight and washed twice in FACS buffer prior to flow cytometry analysis. Proliferation marker levels were quantified in median fluorescence intensity (MFI) and % of cells from intracellular staining flow cytometry.

2.9 B Cell Migration Assay

Bulk splenocytes were isolated following the mouse T cell transduction protocol. Phoenix-ECO stable packaging cells (5e5) in 600μl were seeded in the bottom chamber and waited 2 hours for cells to attach and CXCL13concentration to build up. Pore size of 5μm inserts were placed during the 2 hours waiting time to allow for better cell attachment and spreading. 5μm pore size is typical for B cell migration assay[51]. 5μm is smaller than the diameter of a

typical B cell (7-14μm). This allows for the attracted B cells to extravasate to the bottom chamber[52]. Bulk splenocytes (2e5) splenocytes in 100μl were seeded in the permeable inserts. Waited for 4 hours for attracted CXCR5+ B cells to migrate to the bottom chamber. 600μl media in the bottom chamber were carefully collected without disturbing the attached stable packaging cells. The collected cells were spun and washed with FACS buffer twice. Cells were stained with PE anti-mCD19 for 30 minutes in 4°C then washed twice with FACS buffer prior to flow cytometry analysis.

2.10 Tumor Injection and Imaging

All animal study protocols in this study were previously approved by IACUC. We engrafted 10e6 ID8 tumor in 200μl PBS into each mouse through intraperitoneal (IP) injection one week prior to CAR T cells treatment (2e6)[34]. To image mice weekly, D-luciferin (98mM/mouse) was administered by IP injection. Mice were imaged on IVIS imaging system 7 minutes after luciferin injection. We randomized the mice prior to CAR T cell treatment to achieve similar average luminescence between each group.

3 Results

3.1 Construct Design and Molecular Cloning

A. Human and Mouse CXCL13 Amino Acid Sequence Alignment using NCBI Ortholog Protein Alignment Tool

Fig. 8 | Human and Mouse CXCL13 are Homologous.

Both human and mouse CXCl13 have highly similar amino acid sequence from NCBI ortholog protein alignment tool. And both have similar functions: attracting B cells via CXCR5 receptor. Showing human and mouse CXCL13 have similar structure and functions is important for translational research.

To begin, we first confirmed the similar function of CXCL13 between human and mouse. And the NCBI Ortholog Protein Alignment Tool confirmed the similarity in amino acid sequences of the two proteins **(Fig. 8)**. Human and mouse CXCL13 both attract B cells via CXCR5 receptor[42,49,53].
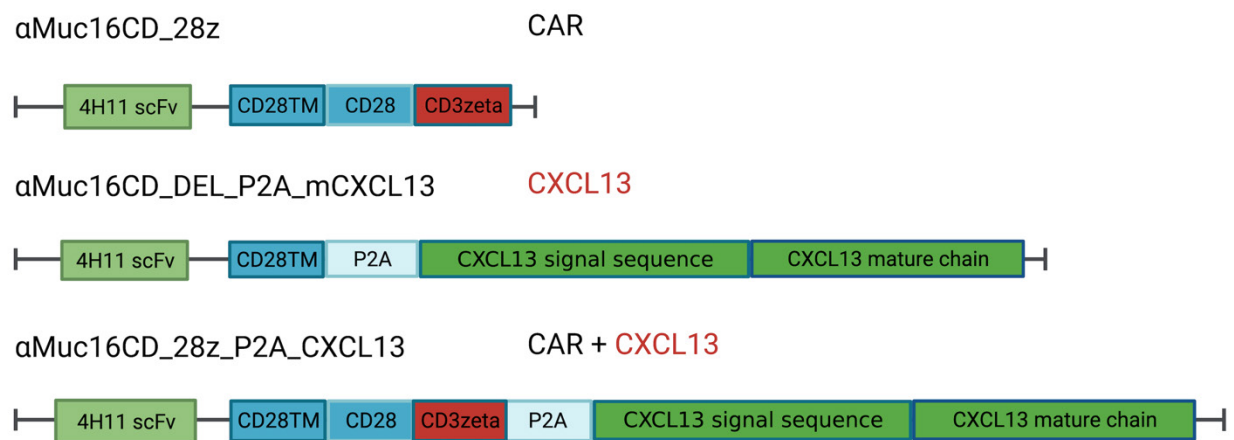

Fig.9 | CAR Structures in This Study

In this study, 3 CARs were included: experimental group, negative control group, and reference group **(Fig. 9)**. CXCL13-armored CAR will be the experimental group. CXCL13-armored DEL CAR will serve as local delivery of CXCL13 and be the negative control group as it does not have CD28 and CD3ζ domains. 2nd generation CAR will be the reference group because this was previously validated in mouse ovarian cancer model. P2A is a ribosomal skipping sequence originally from Porcine Teschovirus[54]. P2A will direct the ribosome to cleave the current reading peptide and synthesize a separate peptide. P2A sequence allows for efficiency expression of multiple proteins on the same vector. For the two CXCL13-

secreting vectors, an endogenous CXCL13 signal sequence was added to ensure the proper secretory trafficking of CXCL13.

We then designed the cloning strategies for constructing CXCL13-secreting CAR and CXCL13-secreting DEL CAR plasmids (**Fig. 10 and 11**). CXCL13-secreting CAR vector was synthesized first and subsequently used as backbone for constructing CXCL13-secreting DEL CAR. We utilized SFG_4H1128z_P2A_CD40L construct as the backbone[55]. To replace the CD40L with CXCL13, we use two restriction enzymes, BstZ17I-HF and XhoI, to digest the backbone. For designing the gblock, we added 20-nucleotide overlaps covering the backbone at both ends for successful Gibson assembly. Gibson assembly was used to insert P2A ribosomal skipping sequence, endogenous CXCL13 signal sequence, and mature chain of CXCL13. After, PCR and gel electrophoresis were performed to validate that the insert had been incorporated into the vector. We then transformed the vector into competent E. coli and plated the transformed E. coli on agarose plate with ampicillin. Two colonies were collected, and PCR was performed to screen for the desired vector. We cultured the colony and purified the DNA using Promega plasmid midiprep system for subsequent Sanger sequencing. We then constructed the CXCL13-secreting DEL CAR vector following the same methods as described above. We developed the cloning strategy for CXCL13-secreting DEL CAR vector based on CXCL13-secreting CAR vector.
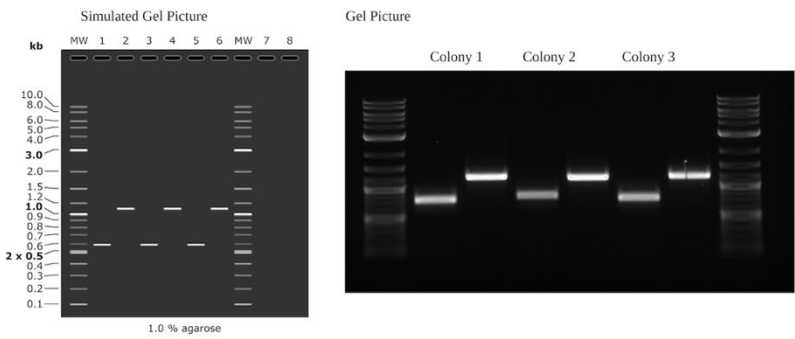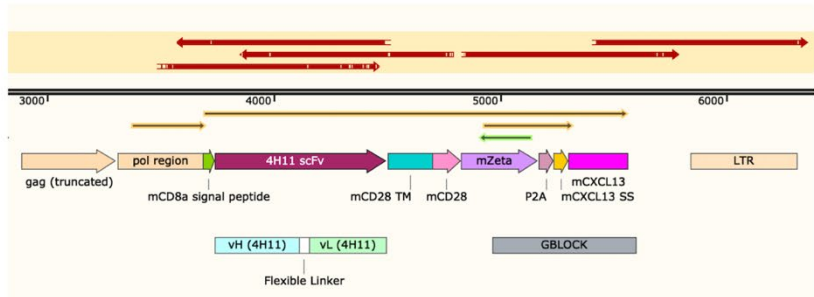
SFG_ αMuc16CD_P2A_CXCL13
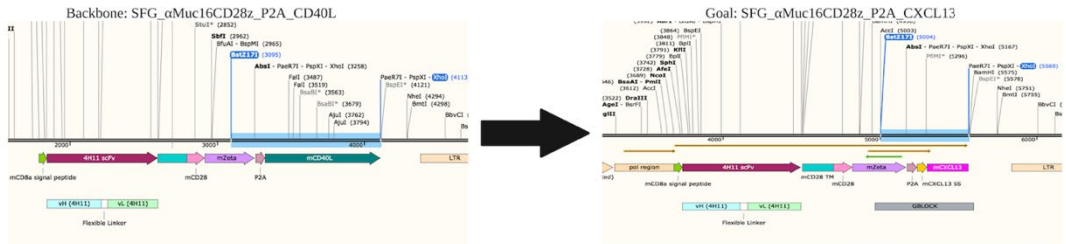
A. Cloning Strategy for Constructing SFG_ αMuc16CD28z_P2A_CXCL13 Plasmid
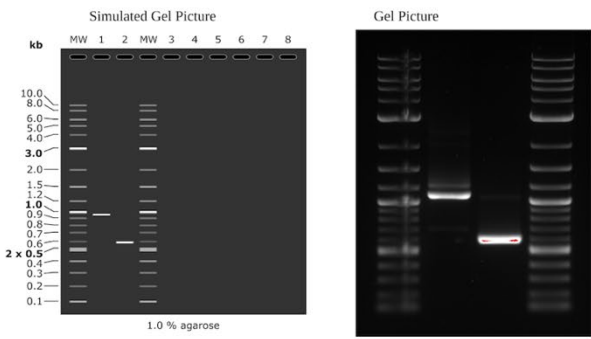
B. PCR Confirmation Test after Gibson Assembly
Lane 2 is SFG_ αMuc16CD28z_P2A _CXCL13. Primers included mCD3z_F and SFG_R3 (586bp)

C. Colony PCR
Primer sets included mCD3z_F & SFG_R3 (586bp) and Mof.SFG.F1 & mCD28TM_R (1095bp)
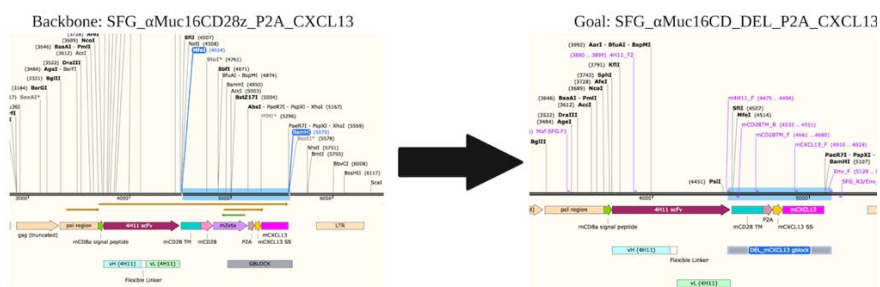

D. Sanger Sequencing alignments on Snapgene
Sanger Sequencing alignments with 5 different primers covering the CAR sequence of the SFG retroviral plasmid

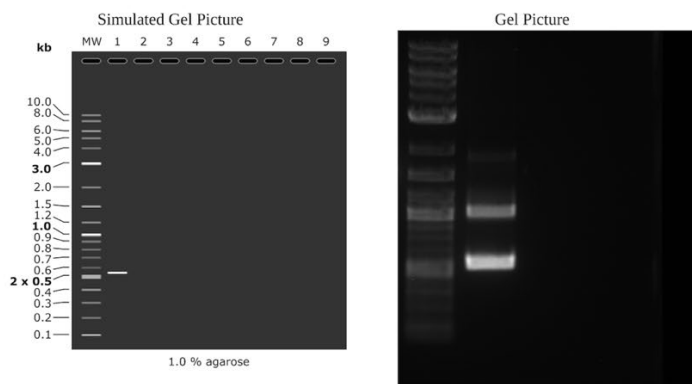**Fig. 10| Successfully Constructed SFG_ αMuc16CD_P2A_CXCL13 Plasmid.**

a, The Cloning Strategy for SFG_ αMuc16CD_P2A_CXCL13. b, PCR confirmation test after gibson assemly. c, Colony PCR. d, Sanger sequencing alignments on Snapgene

We used one primer set to confirm successful integration of the insert to the digested backbone **(Fig. 10b)**. Lane 2 is the construct, SFG_ αMuc16CD_P2A_CXCL13. After confirmed the band has correct size shown by the simulated gel picture, we transform the construct into E. coli and picked 3 colonies to run a colony PCR with two primer sets **(Fig. 10c)**. All three colonies have the expected band sizes (586bp and 1095bp).

SFG_ αMuc16CD _DEL_CXCL13

A. Cloning Strategy for Constructing SFG_ αMuc16CD_DEL_P2A_CXCL13 Plasmid
SFG_ αMuc16CD_CXCL13 was used as backbone. CD28_ CD3ζ_CXCL13 was replaced with DEL_CXCL13 at MfeI and BamHI

B. PCR Confirmation Test after Gibson Assembly
Lane 1 is SFG_ αMuc16CD _DEL_CXCL13. Primers included mCD28TM_F and SFG_R3 (551bp)
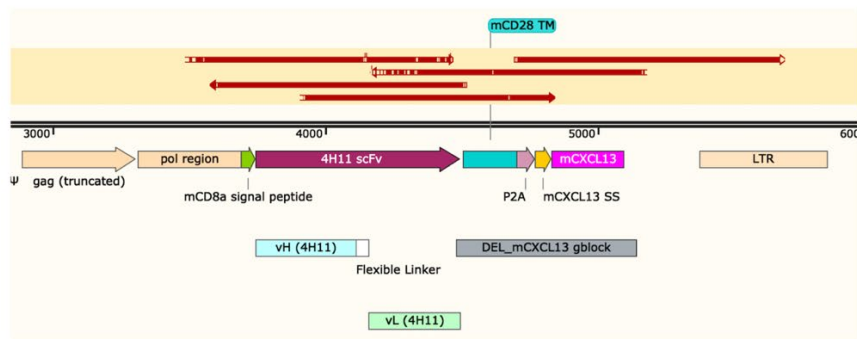
C. Sanger Sequencing alignments on Snapgene
Sanger Sequencing alignments with 5 different primers covering the CAR sequence of the SFG retroviral plasmid

Fig. 11 | Successfully Constructed SFG_ αMuc16CD_P2A_CXCL13 Plasmid.

a, The Cloning Strategy for SFG_ αMuc16CD_DEL_P2A_CXCL13. b, PCR confirmation test after gibson assemly. c, Sanger sequencing alignments on Snapgene.

After successfully making the construct, SFG_ αMuc16CD_P2A_CXCL13, we followed the same protocol to design the cloning strategy of SFG_ αMuc16CD_DEL_P2A_CXCL13 **(Fig. 11a)**. After restriction enzyme digestion and gibson assemly, we run a PCR confirmation test. The gel picture shows two bands due to uncomplet digestion **(Fig. 11b)**. The undigested backbone has a bigger band size because of the remaining CD28 and CD3ζ domains. We picked four colonies and ran a colony PCR.

3.2 DNA Sequencing

After growing up colony, we extracted and purified the plasmid and send it off to AstraZeneca for sanger sequencing. Multiple primers were chosen to ensure that the open reading frame of the CAR can be amplified for Sanger sequencing. The sequence from the plasmid was shown to align the theoretical goal map we designed (**Fig, 10d and 11c**). For CXCL13-secreting CAR, we used with 5 different primers covering the CAR sequence of the SFG retroviral backbone. The red bar alignments match up with the backbone we initially designed on Snapgene. Similarly, we used 5 different primers for Sanger sequencing. And red bar alignments match up with what we designed on Snapgene.

3.3 Transduction of Phoenix-ECO cells

Phoenix-ECO cells are stable retroviral packaging cells used for mouse CAR T cell manufacturing. A detailed schematic of establishing stable packaging cell lines was shown **(Fig. 12a)**. We confirmed the successful transduction and single cell clone collection, and

both stable packaging cell lines have more than 99% transduction efficiency **(Fig. 12b)**. An

example of the gating strategy for transduction check was shown **(Fig. 12c)**.
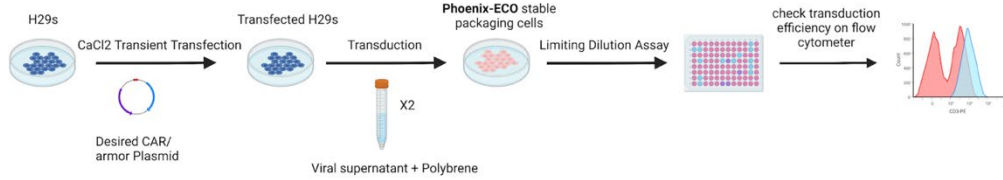
A. Workflow of Manufacturing Stable Packaging Cell Lines
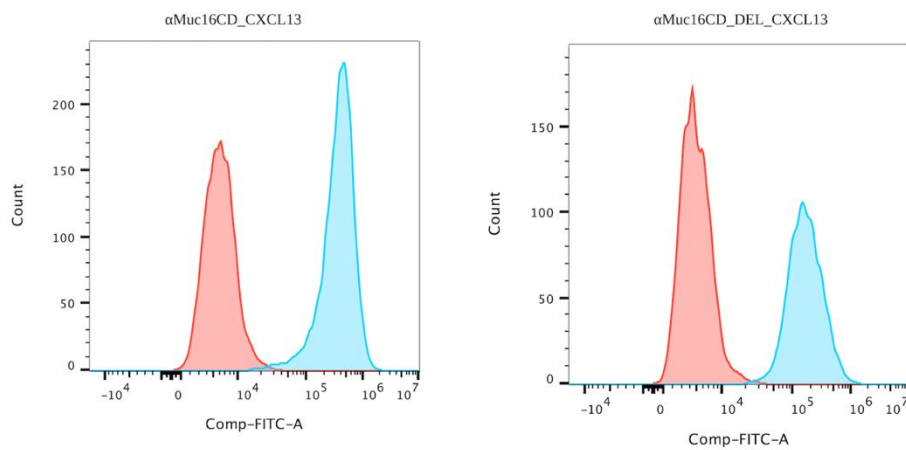
B. Transduction in Phoenix-ECO
Red peak shows Phoenix-ECO empty as negative control. Blue peak shows transduced Phoenix-ECO. Transduction efficiencies are higher than 99% for both constructs.
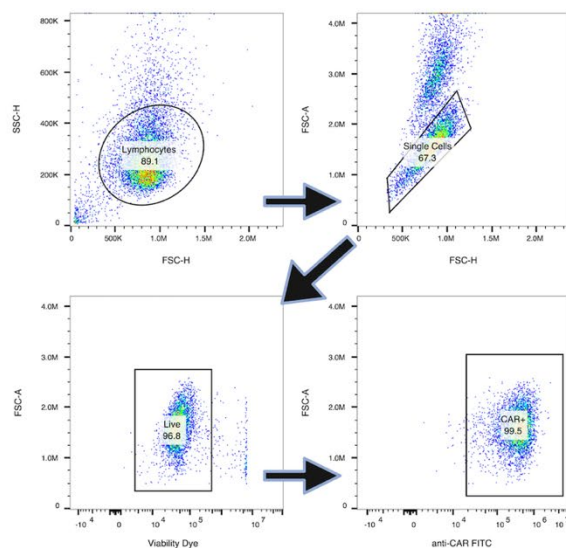
C. Demonstration of Gating Strategy

Fig. 12| Successfully Transduced and Manufactured Phoenix-ECO Stable Packaging Cell Lines for CXCL13-secreting CAR and CXCL13-secreting DEL CAR.

a, The workflow of manufacturing stable packaing cell lines. b, Transduction efficiency of the two stable packaging cell lines shown in histogram. c, Gating strategy.

3.4 Validating the CAR T Cells

After constructing the stable packaging cells needed for CAR T cell manufacturing, we went ahead and transduce mouse T cells for downstream *in vitro* assays. We determined the transduction efficiency on flow cytometer. An example of gating strategy is shown in **Fig. 13a**. The transduction efficiency of the mouse T cells was assessed using anti-CAR antibody, and transduction were all above 80% **(Fig. 13b)**. Detecting transduction with anti-CAR antibody also verifies that CAR is trafficked to cell surface and is being expressed. αMuc16CD_DEL_CXCL13 in **Fig. 13b** was only performed once and more biological replicates are needed for this CAR.

A. Demonstration of Gating Strategy

B. CAR T Cells Viability and Transduction Efficiency
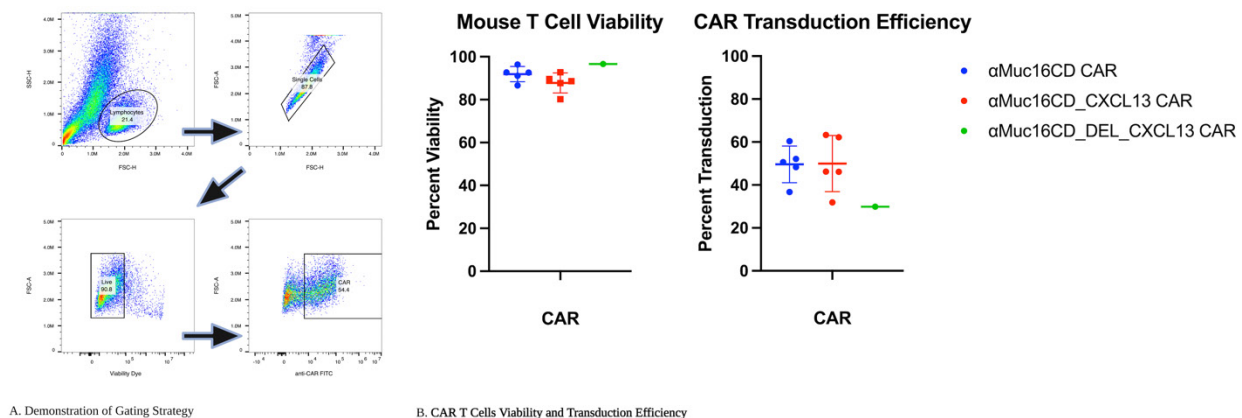
Fig. 13| Transduction efficiency and viability of mouse CAR T cells were consistent.

a, Gating strategy for checking CAR T cell transduction. b, CAR T cell viability and transduction efficiency. Transduction efficiency and viability of mouse CAR T cells were consistent.

3.5 Luciferase-based Cytotoxicity Assay

Cytotoxicity assay aims to validate the function of the CD3ζ domain on the CAR. In **Fig. 14a**, we included three biological replicates at 48-hour timepoint. αMuc16CD CAR and αMuc16CD

_CXCL13 CAR were tested either with or without antigen stimulation. αMuc16CD _CXCL13 CAR performs similar cytotoxicity function compared with αMuc16CD CAR, which is the reference group in this study. In **Fig. 14b**, the cytotoxicity level continues to confirm the similar cytotoxicity function between the two CARs, and the negative control seems to have less background noise.

Both αMuc16CD and αMuc16CD_CXCL13 CARs have similar antigen-specific cytotoxic function, which is expected since two CARs have the same costimulation domain and activation domain. This experiment shows that αMuc16CD_CXCL13 CAR has a functional CD3ζ domain to recognize and kill the antigen-expressing target cells.

A. 48 hours cytotoxicity assay including experimental group, reference group, and negative control

B. 72 hours Cytotoxicity Assay including experimental group, reference group, and negative control
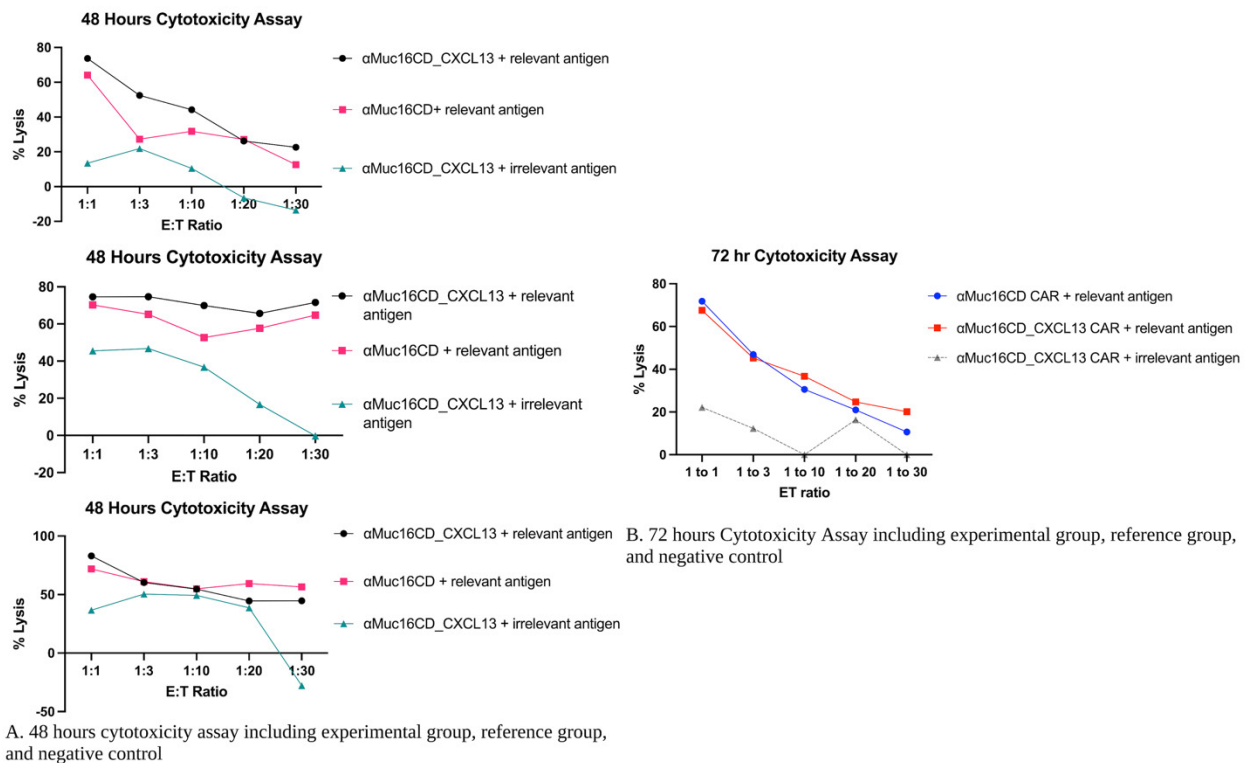
Fig. 14 | αMuc16CD CAR and αMuc16CD_CXCL13 CAR have Similar Antigen-specific Cytotoxicity.

a, 48-hour cytotoxicity assay (n=3). b, 72-hour cytotoxicity assay (n=1).

3.6 Cytokine Assay

After validating the CD3ζ domain on the CAR, we went ahead to validate the cytokine expression. For this experiment, we used intracellular staining flow cytometry to detect the abundance of synthesized cytokines. Fig.13 includes three replicates of the IFN-g level shown either as percent IFN-g+ cells or MFI.

A. % IFNg+ CAR+ Cells   B. IFNg MFI of CAR+ Cells
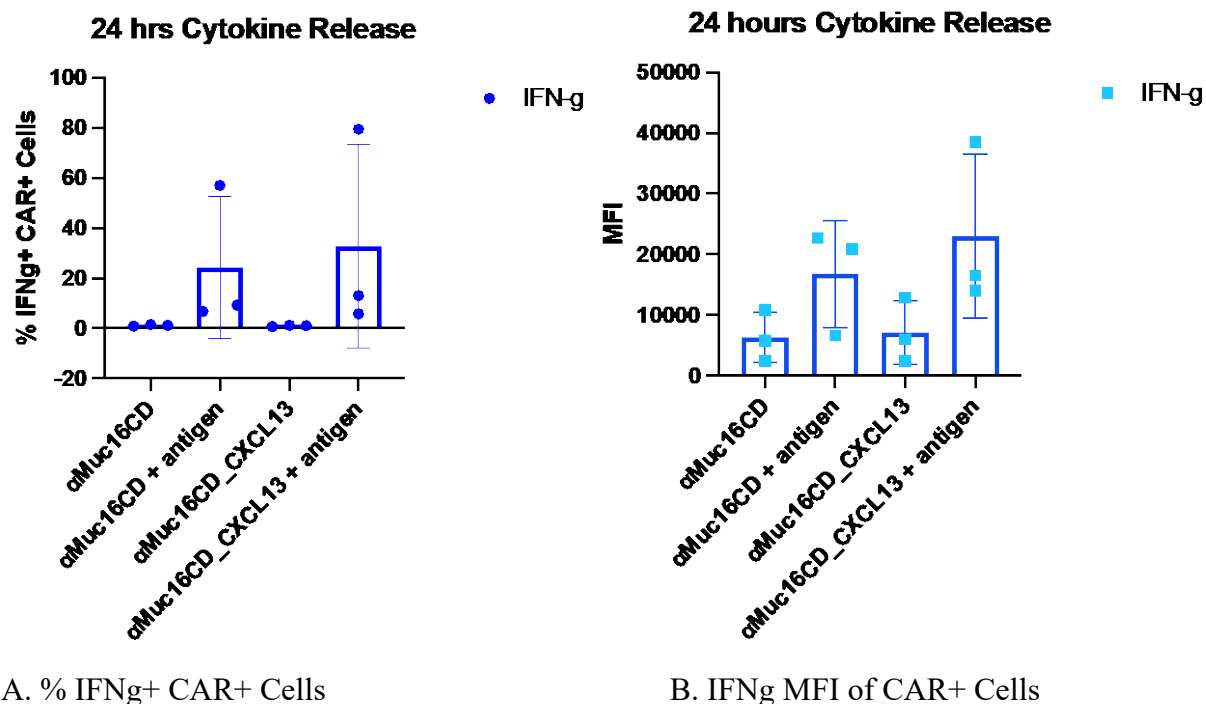
Fig.15 | Cytokine Level inside CAR T Cells with or without Relevant Antigen

Levels of IFNg are shown in two different parameters: the percentage of IFNg+ CAR T cells and MFI of IFNg based off CAR gate **(Fig. 15)**. Overall, current data does show that CAR T cells are activated upon antigen stimulation and αMuc16CD_CXCL13 may secrete more IFNg.

MFI data also shows that αMuc16CD_CXCL13 has more IFNg signal yet statistically insignificant. More replicates are needed to make conclusive judgement of the cytokine levels of the two CARs.

3.7 CD69 Stimulation Assays

After validating the CAR using cytotoxicity assay and cytokine assay, we functionally analyzed the CAR T cells by looking at the activation capacity by CD69 expression, a marker for T cell stimulation. Both percentage of CD69+ cells and MFI based on CAR gate are reported in **Fig. 16b**.
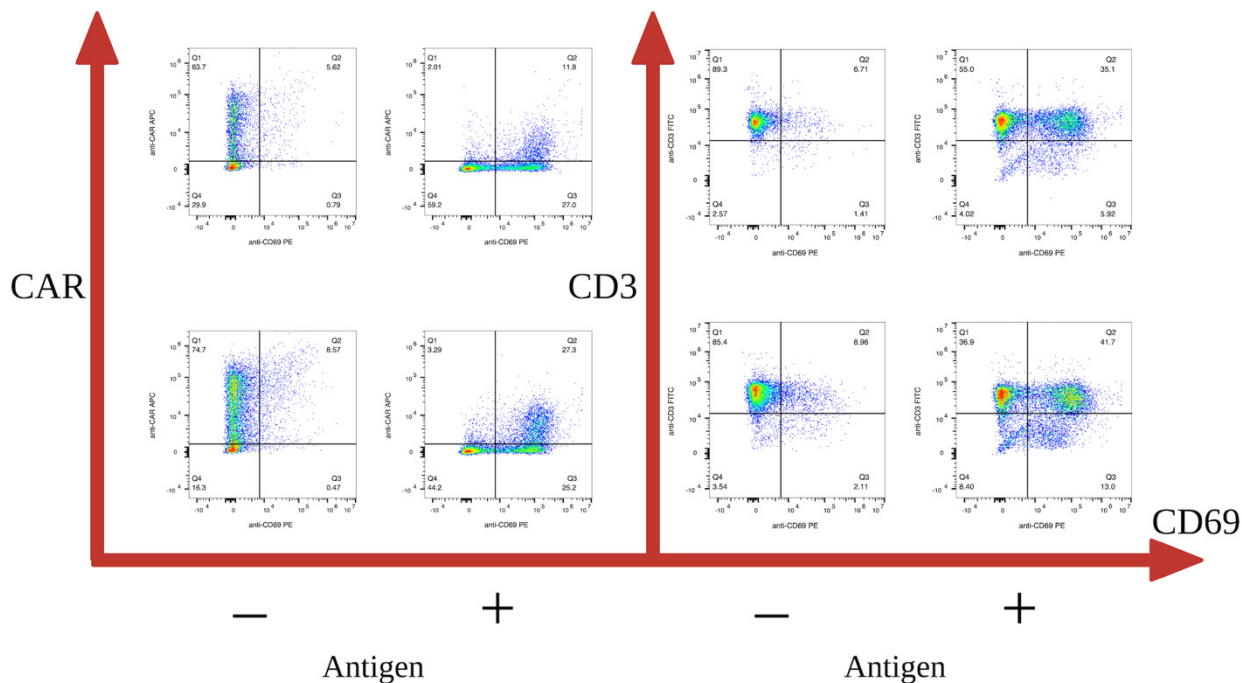
A. Surface Staining: Scatterplot of CD69 expression stratified by CAR and CD3
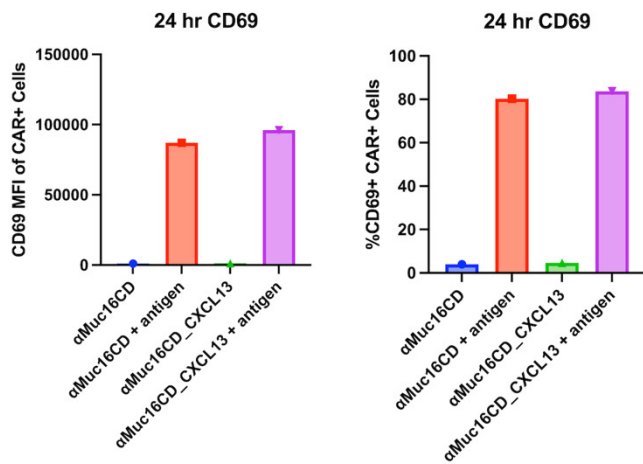
B. CD69 Surface Expression level at 24 hours

Fig. 16| Both CARs are Stimulated upon Antigen Stimulation.

a, Surface staining: scatterplot of CD69 expression stratified by CAR and CD3 gates. b, CD69 surface expression at 24 hours

Fig. 16a shows CAR internalization upon antigen stimulation for 24 hours in surface staining. CARs recycling is a known phenomenon[56]. When CAR T cells are stimulated with antigen, their CARs are being internalized and will eventually recycle back to the cell surface at 48 hours after stimulation. Approximately half of the CAR+ cells internalized their CARs at 24-hour timepoint if we assume CD69+ cells are CAR+ **(Fig. 16a)**. We hypothesized that our CAR T cells have internalized their receptors affecting the accuracy of the CAR+ gate. Even though CAR+ gate might not capture all of the CAR T cells at the timepoint when we analyzed the cells on flow cytometer, we found out that both MFI and percentage based off the CAR+ gate rather than CD3+ gate provide a more robust signal. CAR T cells stimulated with antigen have increased expression level of CD69 **(Fig. 16b)**. Both the MFI and percentage data show that CXCL13-secreting CAR T cells seem to have a higher stimulation level **(Fig. 16b)**. However, to make conclusive judgement, more biological replicates are needed to interpret statistical significance.

3.8 Ki-67 Proliferation Assay

Besides testing the stimulation capacity of mouse CAR T cells, we also tested the proliferative capacity of the mouse CAR T cells upon antigen stimulation. Ki-67 is a nuclear protein which indirectly shows the proliferative state of cells. Both the percentage of Ki-67+ cells and MFI based on CAR gate are reported in **Fig.17b**.
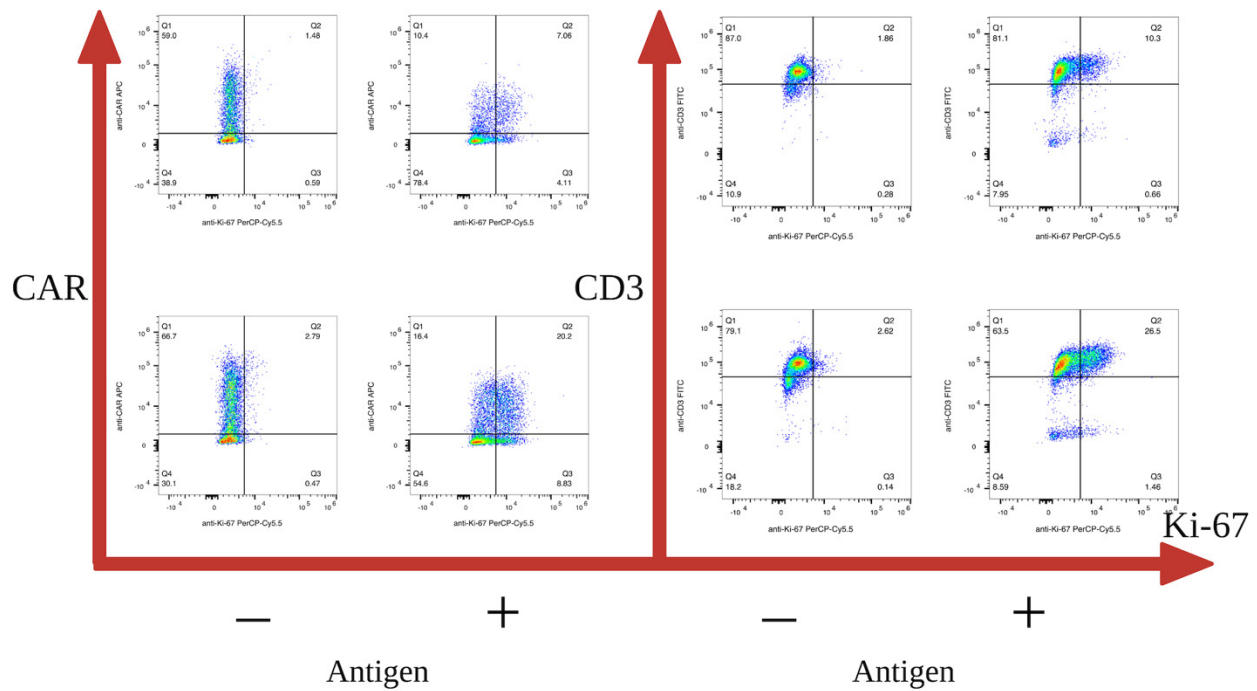
A. Intracellular Staining: Scatterplot of Ki-67 expression stratified by CAR and CD3
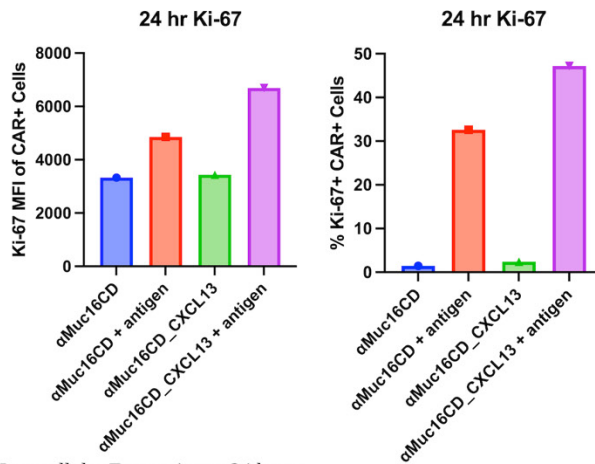
B. Ki-67 Intracellular Expression at 24 hours

Fig. 17 | Both CARs are Proliferating upon Antigen Stimulation.

a, Intracellular staining: scatterplot of Ki-67 expression stratified by CAR and CD3 gates. b, Ki-67 intracellular expression at 24 hours

Since Ki-67 is an intracellular protein inside the nucleus, we performed intracellular staining by first fixing and permeabilizing the cells before antibody staining. Because anti-CAR antibody can easily enter the fixed and permeabilized cells, unlike stimulation assay which

used surface staining, CAR recycling is not a problem in this case for proliferation assay. We therefore reported the MFI and percentage based off CAR+ gate.

We found that αMuc16CD_CXCL13 CAR has a higher signal of Ki-67 compared to that in αMuc16CD CAR in both MFI and percentage parameters **(Fig. 17b)**. This experiment confirmed that αMuc16CD_CXCL13 CAR is functional and seem to have a superior proliferative capacity. Yet, more biological replicates are needed to validate this observation.

3.9 Validation of CXCL13 Expression and Function by Stable Packaging Cells and CAR T cells

We have shown that the CD28 costimulation and CD3ζ domain of the CXCL13-secreting CAR is functional by validating cytotoxicity, cytokine levels, stimulation capacity, and proliferative capacity. It is important to also first validate the secretion and then function of CXCL13.

To validate that CXCL13 is being produced and secreted extracellularly to the media, we collected the supernatant of stable packaging cells and run a mouse CXCL13 ELISA following manufacturer's protocol. The standard curve is reported in **Fig. 18a**. We included two biological replicates for the standard curve and tested three stable packaging cells: αMuc16CD CAR, αMuc16CD_CXCL13 CAR, and αMuc16CD_DEL_CXCL13 CAR **(Fig. 18b)**. We found out that both CXCL13-secreting stable packaging cells are able to secrete significant amount of CXCL13 to the media **(Fig. 18c)**. We noticed that the signal being emitted by conjugated-detection antibody is stronger than the maximal signal the standard curve provides **(Fig. 18c)**. Therefore, an exact amount of CXCL13 in the supernatants cannot be

interpolated. However, ELISA confirms the proper secretion of CXCL13 to the surrounding environment.

A. ELISA Standard Curve

B. Plate Setup
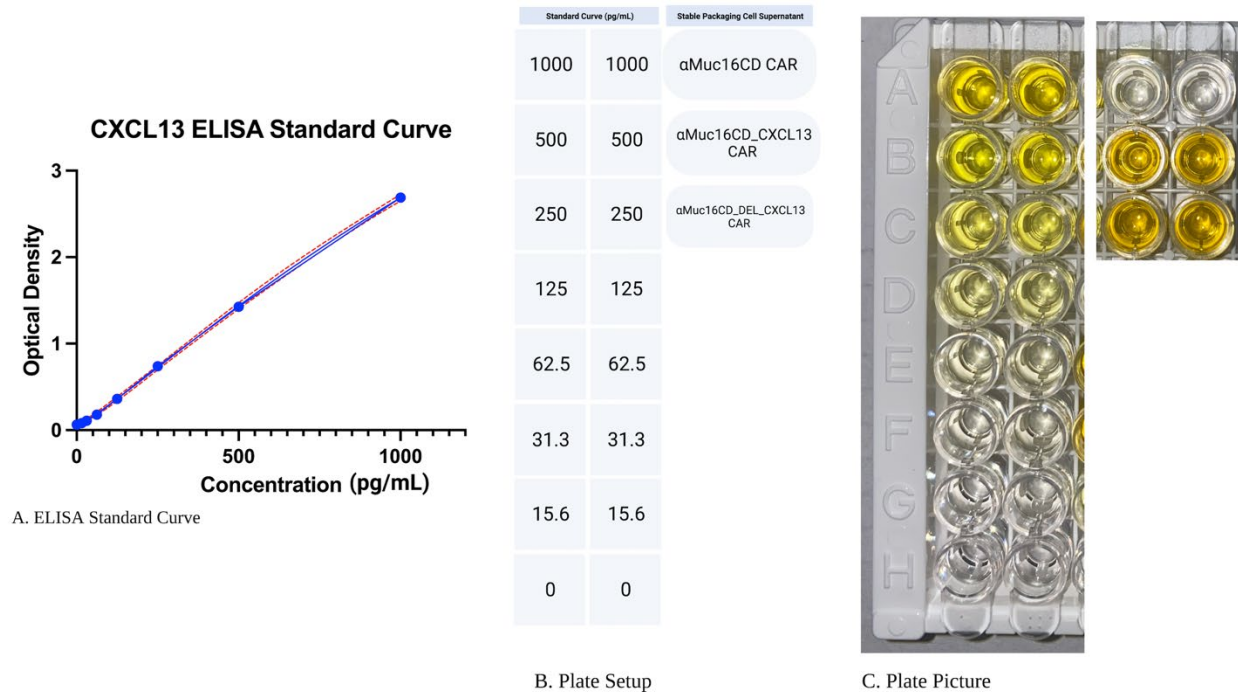
C. Plate Picture

Fig. 18 | CXCL13 Secreted by Stable Packaging Cells is Detectable using ELISA.

a, Standard curve of ELISA. b, Plate setup. c, Actual plate picture showing standard curve (n=2) and supernatants of stable packaing cells (n=1).

We then used a transwell assay to validate the chemoattraction of chemokine CXCL13 from stable packaging cells. **Fig. 19a** details the schematic of a transwell assay. Rather than first isolating CD19+ B cells from the bulk splenocytes, we put bulk splenocytes on the top chamber and use an anti-CD19 antibody to gate out migrated B cells in the bottom chamber on flow cytometer. In **Fig. 19c**, we found that bulk splenocytes treated with ConA and IL-2 expand CXCR5+ CD19+ B cells. Previous research has shown that supernatants of ConA-treated T cells can expand B cells[57]. Therefore, stimulated splenocytes were used for B cell transwell assay. CD19- CXCR5+ cells could potentially be follicular helper T cells **(Fig. 19c)**.

To collect more B cells for downstream assays, we treated the bulk splenocytes following T cell expansion protocol. After waiting for 4 hours allowing for the attracted B cells to migrate, we analyzed percent migrated B cells in bottom chamber and reported the data in **Fig. 19d**.

A. Schematic Diagram of B Cell Migration Assay

B. Gating Strategy of B Cell Migration Assay

C. Bulk Splenocytes Stimulated with ConA and IL-2 have more CXCR5+ CD19+ B Cells

D. Percent of Migrated B Cells in Bottom Chamber
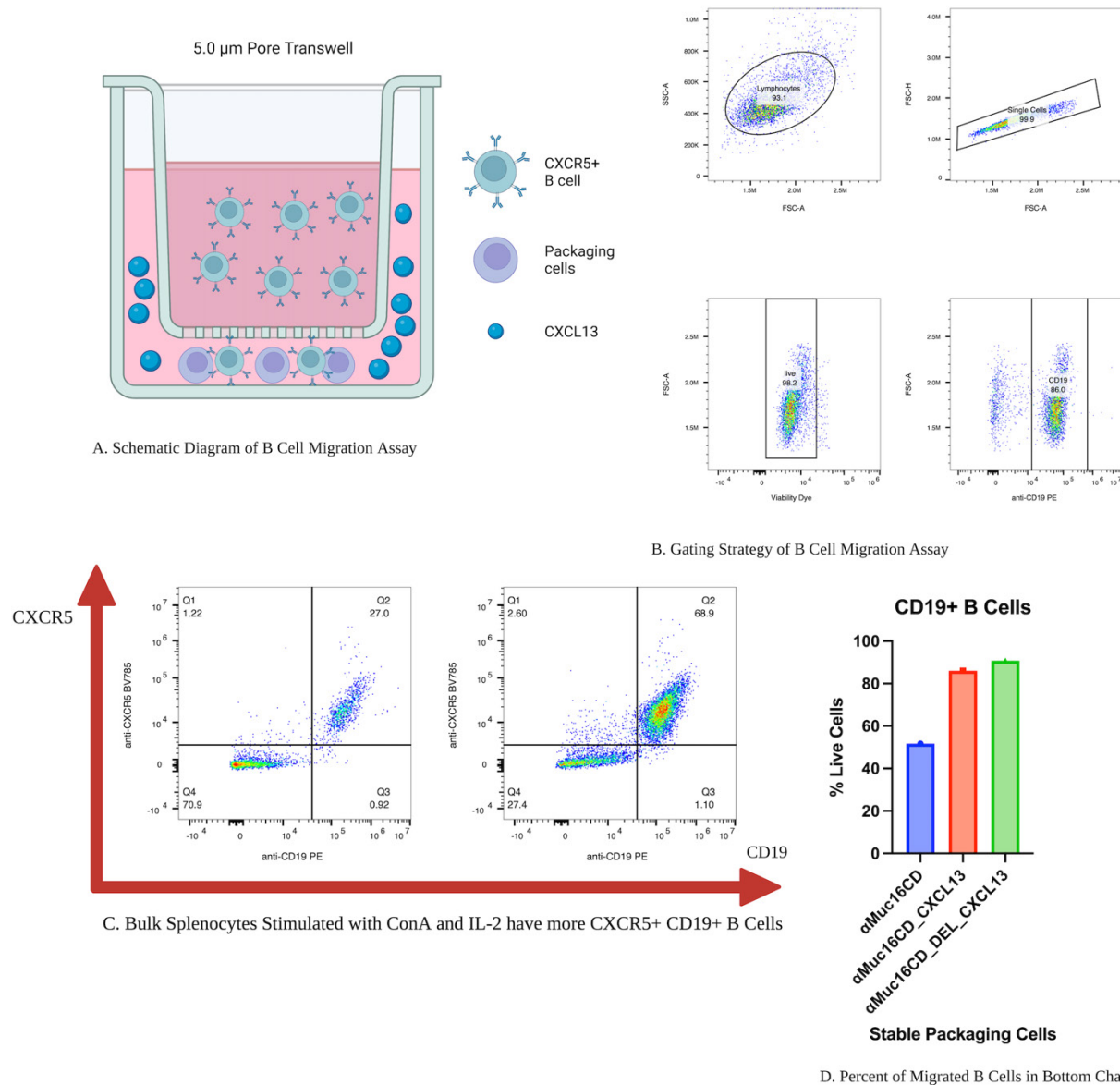
Fig. 19 | CXCL13 Secreted by Stable Packaging Cells is Functional.

a, Schematic of B cell migration assay. b, Gating strategy of B cells. c, Bulk splenocytes stimulated with ConA and IL-2 have more CXCR5+ CD19+ B cells. d, Percent migrated B cells in bottom chamber

In **Fig. 19d**, αMuc16CD CAR is the negative control as it does not secrete CXCL13. Therefore, the migrated B cells in this group is the baseline for B cell migration counts. Both αMuc16CD_CXCL13 and αMuc16CD_DEL_CXCL13 CARs show better B cell chemoattraction. The difference in percentages confirm that the CXCL13 secreted by stable packaging cell lines are capable of attracting CXCR5+ CD19+ B cells.

We have shown that CXCL13 from the stable packaging cells is functional and present. Yet, we also need to prove that CXCL13 can be transduced to the mouse T cells. We confirmed the presence of CXCL13 in transduced mouse CAR T cells on flow cytometer **(Fig. 20)**. Red peak is the αMuc16CD CAR T cells, and blue peak is the αMuc16CD_CXCL13 CAR T cells.
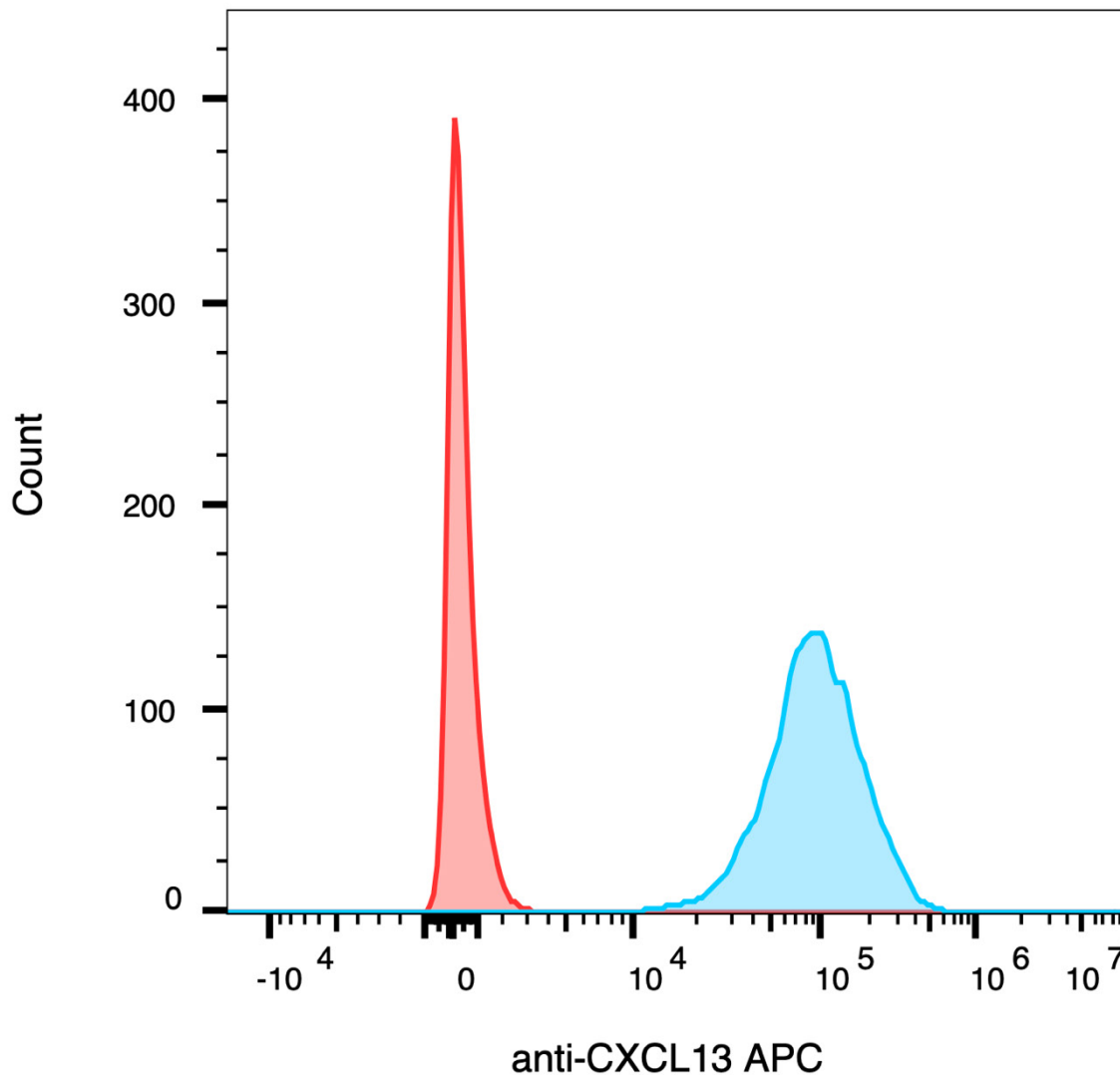
Fig. 20 | CXCL13 is Present in Transduced Mouse CAR T Cells Confirmed by Intracellular Staining Flow Cytometry.

Mouse T cells were collected and fixed/permeabilized for intracellular staining of CXCL13 after T cell transduction. Histogram shows a clear shift in αMuc16CD_CXCL13 population in the channel of APC, which is the fluorophore of the anti-CXCL13 antibody. The armor is expressed inside the T cells.

3.10 *In vivo* Study

After validating the functionality of CAR and CXCL13, we decided to test the anti-tumor function of CXCL13 *in vivo* using an ovarian cancer mouse model. We first injected 10 million ID8 tumor and confirmed successful tumor engraftment by measuring luminescence 1 week after tumor injection **(Fig. 21)**. We then randomized the mice in four groups: untreated group, αMuc16CD CAR group, αMuc16CD_CXCL13 CAR group, and αMuc16CD_DEL_CXCL13 CAR group. We treated the mice with 2 million CAR T cells.
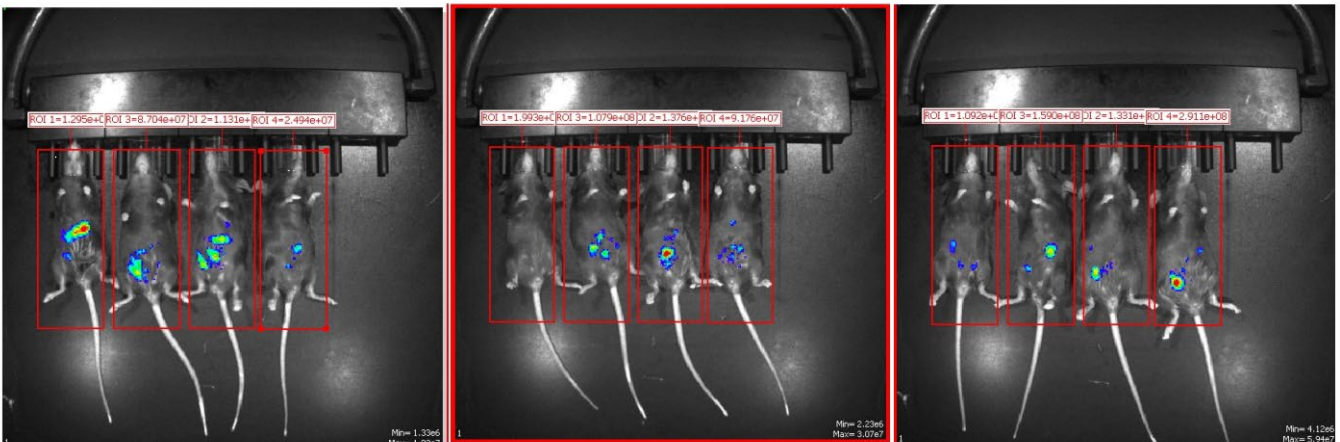
Fig. 21 | Tumor Successfully Engrafted in C57BL/6 Mice.

We randomized the 12mice based on luminescence in 4 conditions: untreated (n=4), αMuc16CD CAR (n=3), αMuc16CD_CXCL13 CAR (n=3), αMuc16CD_DEL_CXCL13 CAR (n=1).

We monitored tumor burden in luminescence weekly until the humane endpoint of this experiment. On day 21 after CAR T cell treatment, we didn't observe any obvious difference in tumor burden across the four groups **(Fig. 22a)**. Currently, nine mice were sacrificed as ascites were developed and affected mice's mobility. Two mice, in total, are still alive: one in αMuc16CD CAR group and the other one in αMuc16CD_CXCL13 CAR group **(Fig. 22b)**.

A. Tumor Burden Measured in Luminescence   B. Kaplan-Meier Survival Analysis
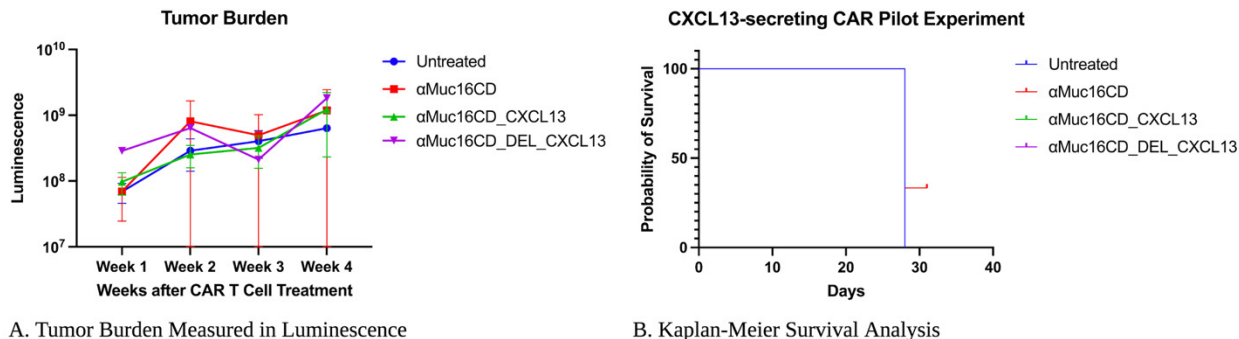
Fig. 22 | Tumor Burden (Luminescence) Remain Similar Across Groups

a, Tumor burden measured in luminescence. b, Kaplan-Meier survival analysis.

In addition to monitoring tumor burden and survival, we were also curious to see if CXCL13 secreted by CAR T cells changes the levels of circulating CXCR5+ B and T cells. We, therefore, collected blood of facial vein from the mice on day 23 **(Fig. 23a)**. We analyzed the percentage of circulating CXCR5+ B and T cells in the periphery. Interesting, we found out that the two groups that secrete CXCL13 in the peritoneal cavity have slightly more CD19+ CXCR5+ live cells in the periphery **(Fig. 23b)**. We also noticed that the percentages of circulating CD3+ live cells remain constant across the four groups **(Fig. 23c)**. However, when we analyzed the percentage of CXCR5+ CD3+ live cells, we found out that αMuc16CD_CXCL13 CAR group has approximately two-fold increase of CXCR5+ CD3+ live cells in the circulating periphery. We hypothesized that CXCL13 in the peritoneal cavity seem to attract CXCR5+ T cells to the periphery. Even though more biological replicates and investigations are required to confirm this hypothesis, this preliminary data shows that CXCL13 could be functional and mobilizing CXCR5+ B and T cells to the periphery and possibly peritoneal cavity.

CD19+ CXCR5+ Cells
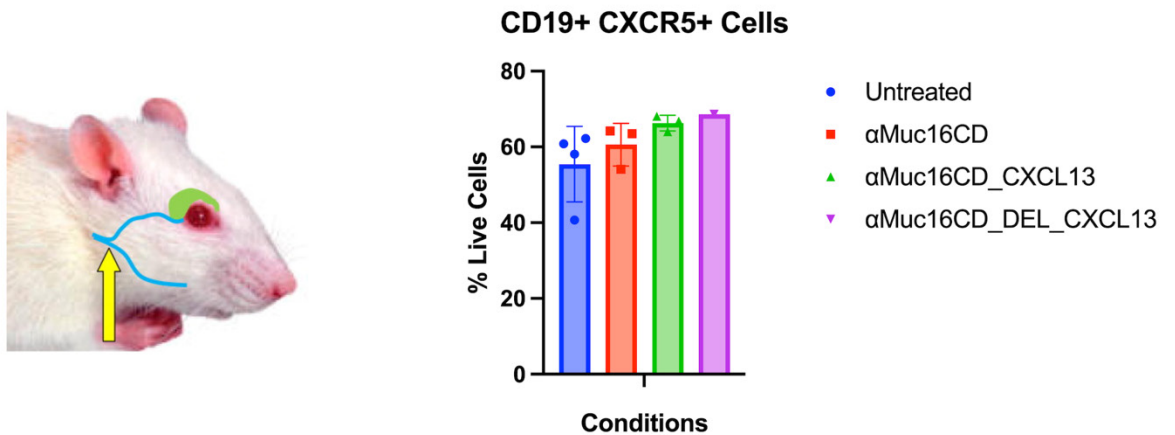
A. Mouse Facial Vein Blood Collection

B. Percent CXCR5+ CD19+ Live Cells in Periphery
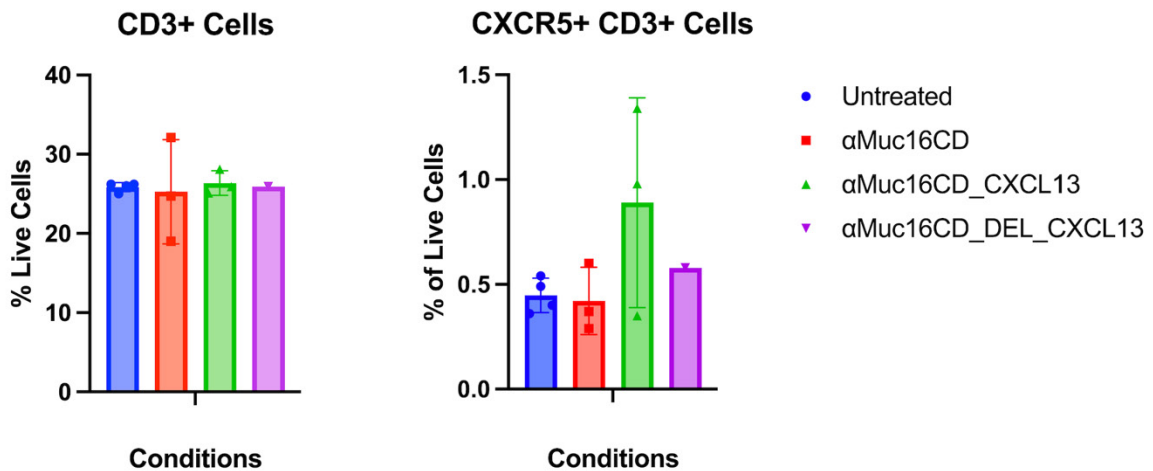
C. Percent CD3+ Live Cells in Periphery

D. Percent CXCR5+ CD3+ Live Cells in Periphery

Fig. 23 | CXCL13 from CAR T Cells Seems to Attract CXCR5+ B and T cells to Periphery.

a, Schematic of facial vein blood collection[58]. b, Percent CXCR5+ CD19+ live cells in periphery. c, Percent CD3+ live cells in periphery. d, Percent CXCR5+ CD3+ live cells in periphery.

4 Discussion

This study aims to test the anti-tumor function of CXCL13 on CAR T cells. We investigated CAR T cells' functionality by looking at the cytotoxic function, cytokine level, proliferation and stimulation capacity. We have so far constructed the needed retroviral plasmid for CAR manufacturing, validated the cytotoxicity of transduced mouse T cells (CD3ζ), confirmed

cytokine production (CD28), stimulation (CD69) and proliferation (Ki-67) capacity. While more replicates are required for rigorous statistical analysis, preliminary data has proven that the αMuc16CD_CXCL13 CAR has proper function comparable to the αMuc16CD CAR. And due to the limited time availability of the project, we decided to move onto a pilot *in vivo* study, which can test the anti-tumor function of CXCL13 in CAR T cells.

Data from cytotoxicity assay shows that αMuc16CD _CXCL13 CAR can be equally as cytotoxic as αMuc16CD CAR **(Fig. 14)**. Having a similar cytotoxic function could mean that CXCL13 is not improving CAR T cell functionality directly by enhancing killing. Data from cytokine assay shows that αMuc16CD _CXCL13 CAR can secrete slightly more IFNg than αMuc16CD CAR when co-culturing with antigen-expressing tumor cells at a 1:1 E:T ratio for 24 hours **(Fig. 15)**. Previous study has shown that a subpopulation of Tfh is capable of secreting IFNg upon antigen stimulation[59]. Another cytokine, IL-2, is a direct indication of the CD28 costimulation domain being stimulated. However, we couldn't find IL-2 using intracellular staining flow cytometry. Thus, secreted IL-2 level in the previously saved supernatant should be quantified either using ELISA or bead-based immunoassay. We plan to run bead-based immunoassay, Luminex, on the supernatants to detect and quantify levels of secreted IL-2. Three replicates of the supernatants were saved from past cytotoxicity experiments.

CXCL13 can not only interact with germinal center B cells in the follicles, it can also interact with both subsets of CD4 and CD8 T cells can express its cognate chemokine receptor, CXCR5. For example, follicular helper T (Tfh) and follicular cytotoxic T cells (Tfc) express CXCR5, importantly, both of which contribute to improved anti-tumor immunity in ovarian cancer

through different mechanisms[60]. Tfh contribute to favorable outcome by activating B cells and inducing TLS in a mouse ovarian cancer model[53]. Tfc is retained in the intratumoral TLS by CXCL13 in high-grade serous ovarian cancer (HGSC) patient samples and contributes to tumor regression in a CD8 T cell-dependent manner in anti-PD-1 therapy[61]. Because both Tfh and Tfc expressing CXCR5 are prognostic markers in ovarian cancer, we hypothesize that CXCL13 might enhance the efficacy of CAR T cells specifically by interacting with the CAR+ Tfh and Tfc. In future studies, it would be interesting to look at the CD4:CD8 ratio and more specifically the percentage of CD4+ CXCR5+ Tfh population.

We reported that αMuc16CD_CXCL13 CAR have slightly enhanced stimulation and proliferative capacity that αMuc16CD CAR **(Fig. 16 and 17)**. The enhanced functionality of αMuc16CD_CXCL13 CAR could be resulted from the CXCR5 signaling. Previous research has shown that CXCR5 can promote the survival and proliferation of cells by activating the PI3K-AKT signaling pathway and MEK-ERK signaling pathway respectively[40]. Our data does indirectly corroborate this concept. However, western blotting experiments are required to confirm the activation of the above-mentioned signaling pathways. To actually confirm that there is a significant difference in the proliferative capacity between the two CARs, more replicates are required.

Furthermore, CXCL13 might also potentially impact the differentiation state of CAR T cells. While the replicative capacity indicated by Ki-67 does not directly link to the stages of T cell differentiation, terminally differentiated T cells that have been expanded more *ex vivo* correlates with poorer persistence and tumor control *in vivo[62].* It is likely that CXCL13 plays

a role on CAR T cells in an autocrine manner that induces a stem cell phenotype. In another study, IL-2 signaling prevents Bcl-6, a key transcription factor for Tfh differentiation, from expressing[63]. And IL-2 also promote T cell exhaustion and Treg differentiation, which impairs the anti-tumor function in CAR T cell therapy[64]. Maybe due to the presence of CXCL13, more Tfhs are differentiated and attracted. This might result in less exhausted CAR T cells and Treg differentiation. Thus, it would be interesting to look at the immunophenotype differences between the two CARs, including the exhaustion markers before and after antigen stimulation.

The ELISA experiment confirmed the proper secretion of CXCL13 **(Fig. 18)**. Transwell experiment data also confirms the proper function of CXCL13 secreted by stable packaging cells **(Fig. 19)**. Stabled packaging cells transduced with CXCL13 transgene can attract more B cells down to the bottom chamber compared to the negative control. Both of these experiments validate the function and secretion of CXCL13, which are pivotal for this project. This, in theory, could also attract more B cells into the local tumor tissue in *in vivo* study. Additionally, the intracellular flow cytometry also confirmed the presence of CXCL13 inside transduced mouse T cells. However, more replicates are needed for calculating statistical significance.

In vivo mouse experiment is currently still ongoing. We injected the tumor and treated the mice with CAR T cells. Tumor burden and survival are monitored weekly until the end of the experiment. While 9 out of 11 mice were sacrificed, and tumor burden is similar across the four groups **(Fig. 22a)**. There are 2 mice that are still alive, and we are hoping to see the

mouse treated with CXCL13-secreting CAR T cells will achieve a longer survival than the mouse treated with conventional CAR T cells **(Fig. 22b)**. Because we could not observe meaning differences for the tumor burden across groups, including not only our experimental group, CXCL13-secreting CAR, but also the 2nd generation CAR, which has been previously validated and successfully tested *in vivo*, this could mean that we injected too much tumor to the extent that the amount of CAR T cells could not successfully control the tumor at a stable level. To further validate the CXCL13-secreting CAR, we should optimize the ID8 model either by engrafting less tumor or treating the mice with more CAR T cells.

While tumor burden and survival analysis do not support CXCL13-secreting CAR T cells have enhanced anti-tumor efficacy yet, interestingly, the blood samples from the mice do indicate that there are slightly more CXCR5+ B and T cells in the periphery **(Fig. 23)**. Since CXCR5+ T cells are prognostic markers in ovarian cancer, increased level of CXCR5+ T cells in the periphery is promising in this pilot study. However, in order to actually validate the presence of attracted CXCR5+ immune cells, solid evidence is required. In the future, we could perform peritoneal wash in treated mice at certain time points. By collecting the peritoneal fluid, we can actually test if there are CXCR5+ immune cells and if CXCL13-secreting CAR T cells correlates with a higher percentage of this types of cells.

5 Future Directions

Future directions of this work are to discern whether CXCL13 can similarly induce TLS and exert similar anti-tumor function in CAR T cell therapy and if CAR T cells armored with CXCL13 can reprogram the immunosuppressive TME in ovarian cancer. However, due to the

limited time span of this study, our current data cannot prove that CXCL13-secreting CAR T cells are able to attract B cells and induce TLS in the peritoneal cavity of mice. To prove that the CXCL13-secreting CAR T cells can induce TLS in mice, IHC analysis staining for CD20+ B cells, CD3+ T cells, and CXCL13 in tumor samples is required to confirm the presence of CXCL13-induced TLS. Even though CXCL13-secreting CAR T cells can likely induce TLS and promote the anti-tumor response, our data does not prove this concept yet.

One of the most important experiments that need to be addressed in future studies is the detection and quantification of anti-tumor antibodies. It remains unknown if CXCL13 improves anti-tumor function only by attracting B cells or also by modulating the functions of CD4 and CD8 T cells. A recent study reported that tumor-specific B cells can promote differentiation of tumor-specific CD4 T follicular helper T cells, which in turn improve the anti-tumor function of CD8 T cells by producing IL-21[65]. Another recent study founded out that a subset of intratumoral PD-1+ CD8+ T cells in patients with non-small-cell lung cancer express significantly more CXCL13 than other CD8 T cells and is a reliable marker to predict response rate of PD-1/PD-L1 treatment[66]. This study reported that CXCL13+ CD8 T cells are usually exhausted and antigen-specific, therefore patients with this group of cell population would benefit the most from checkpoint inhibitors. Yet why exhausted CD8 T cells express more CXCL13 remains unknown. Therefore, CXCL13 might modulate anti-tumor immunity in various ways, and it would be important to elucidate the anti-tumor mechanism of CXCL13 in the context of this study.

To determine if anti-tumor antibodies are being produced by B cells, multiple experiments can be performed: ELISA, flow cytometry, and serum transfer from treated to untreated mice. Because antibodies will have unspecific bindings to tumor cells, a negative control of healthy mice is also required. Asides from detecting anti-tumor antibodies, TLS presence should also be confirmed with IHC. If the anti-tumor function of CXCL13 is contributed by CXCR5+ B cells and their antibodies, we could try anti-CD19 depleting antibody to deplete B cells to see if CXCL13 still play an anti-tumor role. Other immune cell types like macrophage and dendritic cells could also be depleted to see if the anti-tumor function of CXCL13 is contributed by the innate immune system.

Lastly, it would be interesting to combine CXCL13-armored CAR and CD40L-armored CAR together for combined therapy[55]. It is known that CD40L on T cells help to activate B cells[67]. If current study confirms that CXCL13 can attract B cells and induce TLS. An additional CD40L signal given by CAR T cells might further enhance the anti-tumor functions. Yet immunological toxicity might need to be considered because self-reactive B cells might also be attracted and activated by CXCL13 and CD40L signals. The second proposal is to combine checkpoint inhibitors and CXCL13-armored CAR T cell therapy. Because exhausted CD8 T cells express more CXCL13 and can be a reliable marker to predict response of PD-1/PD-L1 therapy, it would be of a great interest to see what will happened if combining both CXCl13-armored CAR and checkpoint inhibitors together.

We have engineered and proven the proper functionality of CXCL13-secreting CAR T cells *in vitro.* Further investigation and optimization of the *in vivo* study is needed to confirm the

anti-tumor function of CXCL13 in ovarian cancer. The concept of engineering CXCL13-

secreting is novel. This study could possibly provide a new perspective for immunotherapy

in ovarian cancer.

References
1.   Cortez AJ, Tudrej P, Kujawa KA, Lisowska KM. Advances in ovarian cancer therapy. *Cancer Chemother Pharmacol*. Jan 2018;81(1):17-38. doi:10.1007/s00280-017-3501-8
2.   Scarlett UK, Conejo-Garcia JR. Modulating the tumor immune microenvironment as an ovarian cancer treatment strategy. *Expert Rev Obstet Gynecol*. Sep 1 2012;7(5):413-419. doi:10.1586/eog.12.41
3.   Lim HJ, Ledger W. Targeted therapy in ovarian cancer. *Womens Health (Lond)*. Jun 2016;12(3):363-78. doi:10.2217/whe.16.4
4.   Bolton KL, Chenevix-Trench G, Goh C, et al. Association between BRCA1 and BRCA2 mutations and survival in women with invasive epithelial ovarian cancer. *JAMA*. Jan 25 2012;307(4):382-90. doi:10.1001/jama.2012.20
5.   Haridas D, Chakraborty S, Ponnusamy MP, et al. Pathobiological implications of MUC16 expression in pancreatic cancer. *PLoS One*. 2011;6(10):e26839. doi:10.1371/journal.pone.0026839
6.   Liu YQ, Wang XL, He DH, Cheng YX. Protection against chemotherapy- and radiotherapy-induced side effects: A review based on the mechanisms and therapeutic opportunities of phytochemicals. *Phytomedicine*. Jan 2021;80:153402. doi:10.1016/j.phymed.2020.153402
7.   Hennecke J, Wiley DC. T cell receptor-MHC interactions up close. *Cell*. Jan 12 2001;104(1):1-4. doi:10.1016/s0092-8674(01)00185-4
8.   Bailey SR, Maus MV. Gene editing for immune cell therapies. *Nat Biotechnol*. Dec 2019;37(12):1425-1434. doi:10.1038/s41587-019-0137-8
9.   Rafiq S, Hackett CS, Brentjens RJ. Engineering strategies to overcome the current roadblocks in CAR T cell therapy. *Nat Rev Clin Oncol*. Mar 2020;17(3):147-167. doi:10.1038/s41571-019-0297-y
10.   Gutcher I, Becher B. APC-derived cytokines and T cell polarization in autoimmune inflammation. *J Clin Invest*. May 2007;117(5):1119-27. doi:10.1172/JCI31720
11.   Bruyns E, Marie-Cardine A, Kirchgessner H, et al. T cell receptor (TCR) interacting molecule (TRIM), a novel disulfide-linked dimer associated with the TCR-CD3-zeta complex, recruits intracellular signaling proteins to the plasma membrane. *J Exp Med*. Aug 3 1998;188(3):561-75. doi:10.1084/jem.188.3.561
12.   Gascoigne NR, Casas J, Brzostek J, Rybakin V. Initiation of TCR phosphorylation and signal transduction. *Front Immunol*. 2011;2:72. doi:10.3389/fimmu.2011.00072
13.   Chen L, Flies DB. Molecular mechanisms of T cell co-stimulation and co-inhibition. *Nat Rev Immunol*. Apr 2013;13(4):227-42. doi:10.1038/nri3405

14.   June CH, Ledbetter JA, Gillespie MM, Lindsten T, Thompson CB. T-cell proliferation involving the CD28 pathway is associated with cyclosporine-resistant interleukin 2 gene expression. *Mol Cell Biol*. Dec 1987;7(12):4472-81. doi:10.1128/mcb.7.12.4472-4481.1987

15.   Li S, Zhang J, Wang M, et al. Treatment of acute lymphoblastic leukaemia with the second generation of CD19 CAR-T containing either CD28 or 4-1BB. *Br J Haematol*. May 2018;181(3):360-371. doi:10.1111/bjh.15195

16.   Cappell KM, Kochenderfer JN. A comparison of chimeric antigen receptors containing CD28 versus 4-1BB costimulatory domains. *Nat Rev Clin Oncol*. Nov 2021;18(11):715-727. doi:10.1038/s41571-021-00530-z

17.   Zhao Z, Condomines M, van der Stegen SJC, et al. Structural Design of Engineered Costimulation Determines Tumor Rejection Kinetics and Persistence of CAR T Cells. *Cancer Cell*. Oct 12 2015;28(4):415-428. doi:10.1016/j.ccell.2015.09.004

18.   Kawalekar OU, RS OC, Fraietta JA, et al. Distinct Signaling of Coreceptors Regulates Specific Metabolism Pathways and Impacts Memory Development in CAR T Cells. *Immunity*. Mar 15 2016;44(3):712. doi:10.1016/j.immuni.2016.02.023

19.   June CH, O'Connor RS, Kawalekar OU, Ghassemi S, Milone MC. CAR T cell immunotherapy for human cancer. *Science*. Mar 23 2018;359(6382):1361-1365. doi:10.1126/science.aar6711

20.   Wang LC, Lo A, Scholler J, et al. Targeting fibroblast activation protein in tumor stroma with chimeric antigen receptor T cells can inhibit tumor growth and augment host immunity without severe toxicity. *Cancer Immunol Res*. Feb 2014;2(2):154-66. doi:10.1158/2326-6066.CIR-13-0027

21.   Moon EK, Wang LC, Dolfi DV, et al. Multifactorial T-cell hypofunction that is reversible can limit the efficacy of chimeric antigen receptor-transduced human T cells in solid tumors. *Clin Cancer Res*. Aug 15 2014;20(16):4262-73. doi:10.1158/1078-0432.CCR-13-2627

22.   Kim R, Emi M, Tanabe K, Arihiro K. Tumor-driven evolution of immunosuppressive networks during malignant progression. *Cancer Res*. Jun 1 2006;66(11):5527-36. doi:10.1158/0008-5472.CAN-05-4128

23.   Jennings MR, Munn D, Blazeck J. Immunosuppressive metabolites in tumoral immune evasion: redundancies, clinical efforts, and pathways forward. *J Immunother Cancer*. Oct 2021;9(10)doi:10.1136/jitc-2021-003013

24.   Yang Y, Yang Y, Yang J, Zhao X, Wei X. Tumor Microenvironment in Ovarian Cancer: Function and Therapeutic Strategy. *Front Cell Dev Biol*. 2020;8:758. doi:10.3389/fcell.2020.00758

25.   Siegel RL, Miller KD, Fuchs HE, Jemal A. Cancer Statistics, 2021. *CA Cancer J Clin*. Jan 2021;71(1):7-33. doi:10.3322/caac.21654

26.   Lengyel E. Ovarian cancer development and metastasis. *Am J Pathol*. Sep 2010;177(3):1053-64. doi:10.2353/ajpath.2010.100105

27.   Kenny HA, Chiang CY, White EA, et al. Mesothelial cells promote early ovarian cancer metastasis through fibronectin secretion. *J Clin Invest*. Oct 2014;124(10):4614-28. doi:10.1172/JCI74778

28.   Mei S, Chen X, Wang K, Chen Y. Tumor microenvironment in ovarian cancer peritoneal metastasis. *Cancer Cell Int*. Jan 25 2023;23(1):11. doi:10.1186/s12935-023-02854-5

29.   Oza AM, Cook AD, Pfisterer J, et al. Standard chemotherapy with or without bevacizumab for women with newly diagnosed ovarian cancer (ICON7): overall survival results of a phase 3 randomised trial. *Lancet Oncol*. Aug 2015;16(8):928-36. doi:10.1016/S1470-2045(15)00086-8

30.   Gonzalez-Martin A, Pothuri B, Vergote I, et al. Niraparib in Patients with Newly Diagnosed Advanced Ovarian Cancer. *N Engl J Med*. Dec 19 2019;381(25):2391-2402. doi:10.1056/NEJMoa1910962

31.   Felder M, Kapur A, Gonzalez-Bosquet J, et al. MUC16 (CA125): tumor biomarker to cancer therapy, a work in progress. *Mol Cancer*. May 29 2014;13:129. doi:10.1186/1476-4598-13-129

32.   Das S, Majhi PD, Al-Mugotir MH, Rachagani S, Sorgen P, Batra SK. Membrane proximal ectodomain cleavage of MUC16 occurs in the acidifying Golgi/post-Golgi compartments. *Sci Rep*. Jun 5 2015;5:9759. doi:10.1038/srep09759

33.   Koneru M, Purdon TJ, Spriggs D, Koneru S, Brentjens RJ. IL-12 secreting tumor-targeted chimeric antigen receptor T cells eradicate ovarian tumors in vivo. *Oncoimmunology*. Mar 2015;4(3):e994446. doi:10.4161/2162402X.2014.994446

34.   Rafiq S, Yeku OO, Jackson HJ, et al. Targeted delivery of a PD-1-blocking scFv by CAR-T cells enhances anti-tumor efficacy in vivo. *Nat Biotechnol*. Oct 2018;36(9):847-856. doi:10.1038/nbt.4195

35.   Kuhn NF, Purdon TJ, van Leeuwen DG, et al. CD40 Ligand-Modified Chimeric Antigen Receptor T Cells Enhance Antitumor Function by Eliciting an Endogenous Antitumor Response. *Cancer Cell*. Mar 18 2019;35(3):473-+. doi:10.1016/j.ccell.2019.02.006

36.   Hughes CE, Nibbs RJB. A guide to chemokines and their receptors. *FEBS J*. Aug 2018;285(16):2944-2971. doi:10.1111/febs.14466

37.   von Hundelshausen P, Agten SM, Eckardt V, et al. Chemokine interactome mapping enables tailored intervention in acute and chronic inflammation. *Sci Transl Med*. Apr 5 2017;9(384)doi:10.1126/scitranslmed.aah6650

38.   Miller MC, Mayo KH. Chemokines from a Structural Perspective. *Int J Mol Sci*. Oct 2 2017;18(10)doi:10.3390/ijms18102088

39.   Muller G, Lipp M. Signal transduction by the chemokine receptor CXCR5: structural requirements for G protein activation analyzed by chimeric CXCR1/CXCR5 molecules. *Biol Chem*. Sep 2001;382(9):1387-97. doi:10.1515/BC.2001.171

40.   Kazanietz MG, Durando M, Cooke M. CXCL13 and Its Receptor CXCR5 in Cancer: Inflammation, Immune Response, and Beyond. *Front Endocrinol (Lausanne)*. 2019;10:471. doi:10.3389/fendo.2019.00471

41.   Schumacher TN, Thommen DS. Tertiary lymphoid structures in cancer. *Science*. Jan 7 2022;375(6576):eabf9419. doi:10.1126/science.abf9419

42.   Ukita M, Hamanishi J, Yoshitomi H, et al. CXCL13-producing CD4+ T cells accumulate in the early phase of tertiary lymphoid structures in ovarian cancer. *JCI Insight*. Jun 22 2022;7(12)doi:10.1172/jci.insight.157215

43.   Fridman WH, Meylan M, Petitprez F, Sun CM, Italiano A, Sautes-Fridman C. B cells and tertiary lymphoid structures as determinants of tumour immune contexture and clinical outcome. *Nat Rev Clin Oncol*. Jul 2022;19(7):441-457. doi:10.1038/s41571-022-00619-z

44.   Meylan M, Petitprez F, Becht E, et al. Tertiary lymphoid structures generate and propagate anti-tumor antibody-producing plasma cells in renal cell cancer. *Immunity*. Mar 8 2022;55(3):527-541 e5. doi:10.1016/j.immuni.2022.02.001

45.   Fridman WH, Petitprez F, Meylan M, et al. B cells and cancer: To B or not to B? *J Exp Med*. Jan 4 2021;218(1)doi:10.1084/jem.20200851

46.   Cabrita R, Lauss M, Sanna A, et al. Tertiary lymphoid structures improve immunotherapy and survival in melanoma. *Nature*. Jan 2020;577(7791):561-565. doi:10.1038/s41586-019-1914-8

47.   Sorin M, Karimi E, Rezanejad M, et al. Single-cell spatial landscape of immunotherapy response reveals mechanisms of CXCL13 enhanced antitumor immunity. *J Immunother Cancer*. Feb 2023;11(2)doi:10.1136/jitc-2022-005545

48.   Kroeger DR, Milne K, Nelson BH. Tumor-Infiltrating Plasma Cells Are Associated with Tertiary Lymphoid Structures, Cytolytic T-Cell Responses, and Superior Prognosis in Ovarian Cancer. *Clin Cancer Res*. Jun 15 2016;22(12):3005-15. doi:10.1158/1078-0432.CCR-15-2762

49.   Luther SA, Lopez T, Bai W, Hanahan D, Cyster JG. BLC expression in pancreatic islets causes B cell recruitment and lymphotoxin-dependent lymphoid neogenesis. *Immunity*. May 2000;12(5):471-81. doi:10.1016/s1074-7613(00)80199-5

50.   Swift S, Lorens J, Achacoso P, Nolan GP. Rapid production of retroviruses for efficient gene delivery to mammalian cells using 293T cell-based systems. *Curr Protoc Immunol*. May 2001;Chapter 10:Unit 10 17C. doi:10.1002/0471142735.im1017cs31

51.   Moratz C, Kehrl JH. In vitro and in vivo assays of B-lymphocyte migration. *Methods Mol Biol*. 2004;271:161-71. doi:10.1385/1-59259-796-3:161

52.   Opstelten D, Osmond DG. Pre-B cells in mouse bone marrow: immunofluorescence stathmokinetic studies of the proliferation of cytoplasmic mu-chain-bearing cells in normal mice. *J Immunol*. Dec 1983;131(6):2635-40.

53.   Chaurio RA, Anadon CM, Lee Costich T, et al. TGF-beta-mediated silencing of genomic organizer SATB1 promotes Tfh cell differentiation and formation of intra-tumoral tertiary lymphoid structures. *Immunity*. Jan 11 2022;55(1):115-128 e9. doi:10.1016/j.immuni.2021.12.007

54.   Kim JH, Lee SR, Li LH, et al. High cleavage efficiency of a 2A peptide derived from porcine teschovirus-1 in human cell lines, zebrafish and mice. *PLoS One*. 2011;6(4):e18556. doi:10.1371/journal.pone.0018556

55.   Kuhn NF, Purdon TJ, van Leeuwen DG, et al. CD40 Ligand-Modified Chimeric Antigen Receptor T Cells Enhance Antitumor Function by Eliciting an Endogenous Antitumor Response. *Cancer Cell*. Mar 18 2019;35(3):473-488 e6. doi:10.1016/j.ccell.2019.02.006

56.   Chapman NM, Gottschalk S, Chi H. Preventing Ubiquitination Improves CAR T Cell Therapy via 'CAR Merry-Go-Around'. *Immunity*. Aug 18 2020;53(2):243-245. doi:10.1016/j.immuni.2020.07.023

57.   Moller SA, Danielsson L, Borrebaeck CA. Concanavalin A-induced B-cell proliferation mediated by allogeneically derived helper factors. *Immunology*. Mar 1986;57(3):387-93.

58.   Joslin JO. Blood Collection Techniques in Exotic Small Mammals. *J Exot Pet Med*. Apr 2009;18(2):117-139. doi:10.1053/j.jepm.2009.04.002

59.   Fang D, Cui K, Mao K, et al. Transient T-bet expression functionally specifies a distinct T follicular helper subset. *J Exp Med*. Nov 5 2018;215(11):2705-2714. doi:10.1084/jem.20180927

60.   E J, Yan F, Kang Z, Zhu L, Xing J, Yu E. CD8(+)CXCR5(+) T cells in tumor-draining lymph nodes are highly activated and predict better prognosis in colorectal cancer. *Hum Immunol*. Jun 2018;79(6):446-452. doi:10.1016/j.humimm.2018.03.003

61.   Yang M, Lu J, Zhang G, et al. CXCL13 shapes immunoactive tumor microenvironment and enhances the efficacy of PD-1 checkpoint blockade in high-grade serous ovarian cancer. *J Immunother Cancer*. Jan 2021;9(1)doi:10.1136/jitc-2020-001136

62.   Kouro T, Himuro H, Sasada T. Exhaustion of CAR T cells: potential causes and solutions. *J Transl Med*. May 23 2022;20(1):239. doi:10.1186/s12967-022-03442-3

63.   Johnston RJ, Choi YS, Diamond JA, Yang JA, Crotty S. STAT5 is a potent negative regulator of TFH cell differentiation. *J Exp Med*. Feb 13 2012;209(2):243-50. doi:10.1084/jem.20111174

64.   Sim GC, Martin-Orozco N, Jin L, et al. IL-2 therapy promotes suppressive ICOS+ Treg expansion in melanoma patients. *J Clin Invest*. Jan 2014;124(1):99-110. doi:10.1172/JCI46266

65.   Cui C, Wang J, Fagerberg E, et al. Neoantigen-driven B cell and CD4 T follicular helper cell collaboration promotes anti-tumor CD8 T cell responses. *Cell*. Dec 9 2021;184(25):6101-6118 e13. doi:10.1016/j.cell.2021.11.007

66.   Thommen DS, Koelzer VH, Herzig P, et al. A transcriptionally and functionally distinct PD-1(+) CD8(+) T cell pool with predictive potential in non-small-cell lung cancer treated with PD-1 blockade. *Nat Med*. Jul 2018;24(7):994-1004. doi:10.1038/s41591-018-0057-z

67.   Elgueta R, Benson MJ, de Vries VC, Wasiuk A, Guo YX, Noelle RJ. Molecular mechanism and function of CD40/CD40L engagement in the immune system. *Immunological Reviews*. May 2009;229:152-172. doi:10.1111/j.1600-065X.2009.00782.x